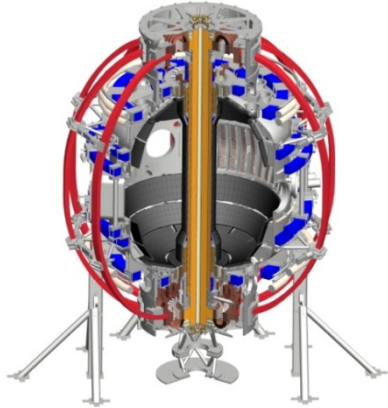


Chapter 2



Research Goals and Plans for Macroscopic Stability

To do:

- Replace the figures above with something representative of your chapter
- Incorporate comments from PAC report
- Make sure all figure and section numbers are correct.

2.1 Overview of goals and plans

2.1.1 Establish predictive capability for the sustained stability of high performance FNSF, ST Pilot, and ITER plasmas

(Add text here)

2.1.2 Thrusts and goals by topical area

2.1.2.1 Understand and advance passive and active feedback control to sustain macroscopic stability

Global MHD instabilities (such as the kink/ballooning mode, and resistive wall mode (RWM)) are critically important to avoid or control as they lead to plasma disruption, terminating the discharge and leading to large, potentially damaging electromagnetic forces and heat loads on the structure of fusion producing devices.

While many targeted performance parameters have been reached in world tokamaks, such plasmas will need to be sustained for far longer pulse lengths in machines such as FNSF, ITER, and DEMO than have been produced to date. Research has therefore changed focus to examine sustained global mode stability over long pulses and to examine profile evolution for routine long pulse operation at high beta and at high non-inductive current fraction. Common to the following studies is the unique physics understanding and control ramifications that come from such operation, and the understanding and prediction of the effect of excursions from this condition due to transient behavior. It is especially important to realize that plasma operation under marginal stability points (set, for example by plasma beta, internal inductance, rotation) is insufficient to ensure disruption-free, continuous operation in either ITER inductive or advanced scenarios due to these transients in plasma profiles. Such transients can rapidly change a stable operational point to an unstable plasma state. Therefore, understanding plasma stability gradients vs. key profiles affecting stability is essential for all operational states in ITER.

NSTX-U will provide key capabilities for critical physics understanding based on present research in plasma operation regimes applicable to ITER and future magnetic fusion devices. NSTX-U will be unique in its operation in non-inductively driven plasmas. This major operational regime for NSTX-U, which may require greater control, provides a unique lab to test advanced stability physics. Additionally, NSTX-U will operate in the unique high beta ST operational space, which will allow performance of advanced stability control in an operating space where disruptivity is not maximized at the highest β_N , or β_N/I_i .

With significantly expanded profile control capabilities (e.g. q, plasma rotation), NSTX-U will allow greater ability to perturb these important profiles for investigations of how to prevent plasma disruptions excited from such excursions. Research on such disruption prevention will be conducted as a combination of active mode control and active profile control. Instability onset leading to modes growing on a relatively fast RWM growth time (milliseconds) will be actively controlled by an expanded RWM state space controller on NSTX-U, while concurrent active control of q and plasma rotation profile working on slower timescales (~50 – 100ms) will move the plasma back into a stable region. This will allow active mode control to be used transiently, which will reduce power needs, and will test the coupling of these two control techniques.

2.1.2.2 Understand 3D field effects and provide physics basis for optimizing stability through equilibrium profile control by 3D fields

Tokamaks are sensitive to a small non-axisymmetric (3D) field. A small 3D field almost always exists due to imperfect primary magnets and can cause unnecessary transport, instability, and even can lead to a disruption if not properly compensated. On the other hand, 3D fields can provide additional knobs for stability control, by producing non-ambipolar transport locally and modifying equilibrium profiles, as well known by edge localized mode (ELM) control using resonant magnetic fields and resistive wall mode (RWM) control using non-resonant magnetic fields. An important question is how to achieve the controllability as well as the predictability of these 3D field applications to improve tokamak performance.

There has been substantial progress in understanding of 3D field effects. Research on $n=1$ error field correction in NSTX highlighted the importance of plasma response [1], and successful $n=3$ non-resonant error field correction was validated across theory and experiment and has been routinely used to maximize the toroidal angular momentum [2]. Reliable error field correction will be much more important in the next-step devices such as FNSF, ST Pilot, and ITER, as a disruption by error-field-driven locking would be detrimental to plasma facing components. The $n=1$ error field correction method developed in NSTX and by IPEC has been actively applied to ITER [3] and is changing the paradigm of the error field correction. Also, the study of magnetic braking in NSTX successfully showed the importance of neoclassical toroidal viscosity (NTV) physics in tokamaks [4] and now magnetic braking is ubiquitous for toroidal rotation control in other tokamaks. Magnetic braking will be an essential tool to control the toroidal rotation and thereby suppress various instabilities in next-step devices, but the NTV physics behind it is highly complex, depending on regimes. Nonetheless many essential features of NTV physics have been theoretically understood [5], numerically verified [6,7], and partially validated from various experiments. Another well-known effect of 3D fields is local modification of transport and stability, either by non-ambipolar transport or by stochastic transport with magnetic islands. Although this is demonstrated by RMP ELM suppression in DIII-D, NSTX $n=3$ applications showed another possible 3D field effect by triggering ELMs rather than mitigating ELMs. All of this evidence indicates the powerful utility of 3D fields, but at the same time the complex interaction between 3D fields and tokamak plasmas, and thus substantial research activities are still required.

NSTX-U can provide a highly relevant environment for 3D field research. Collisionality is one of the most important parameters to govern 3D field physics, and the low collisionality regime relevant for the next-step devices should be carefully and fully explored. NSTX-U aims for higher temperature and low density operation, which will result in much lower collisionality. The 6 independent switching power amplifiers (SPAs) will give more flexibility in field spectrum.

The upgraded SPAs will enable us to study non-resonant error field effects on resonant error field correction, and to control toroidal rotation through magnetic braking while applying RWM and dynamic error field correction. The toroidal rotation profile will also be more flexible because of the 2nd off-axis NBI system. The combination of the new NBIs and the upgraded SPAs will provide various possibilities of toroidal momentum and rotation profile control, as well as equilibrium control in general, in unexplored parametric regime. Furthermore, the non-axisymmetric control coil (NCC) will give unprecedented flexibility in 3D field studies, with two rows of coils that can produce static fields up to $n=6$ and rotating fields up to $n=4$. The poloidal field spectrum will also be as rich as the ITER RMP coils, if combined with the present RWMEF coil at the midplane and with the 6 power supplies in total. In summary, the 5-year research in NSTX-U with the new NBI, SPAs, NCC, and with upgraded diagnostic systems will be able to greatly improve understanding and predictability of 3D field effects and ultimately the required controllability for next-step devices such as FNSF, ST Pilot, and ITER.

2.1.2.3 Understand disruption dynamics and develop techniques on disruption detection, mitigation, and avoidance, in high-performance ST plasmas

(Add text here)

2.2 Research Plans

2.2.1 Thrust 1 – Understand and advance passive and active feedback control to sustain macroscopic stability

2.2.1.1 Year 1 of NSTX-U operation

2.2.1.1.1 Recover and explore NSTX MS control capabilities on stability

NSTX-U will begin operation with a different plasma shape, aspect ratio, and control capabilities than NSTX. This includes independent operation of all six control coils, rather than in three pairs. It is essential to the NSTX-U mission that macroscopic control capabilities that enable high performance operation be recovered. A campaign of exploration of feedback gains, phases and other settings that allow high performance will therefore be necessary.

2.2.1.1.2 Assess the β or q limit with new shaping control and off-axis NBCD

Two other advances that will make NSTX-U different than NSTX are new shaping control techniques and the new off-axis neutral beam. Using these tools, a new space of beta and q -

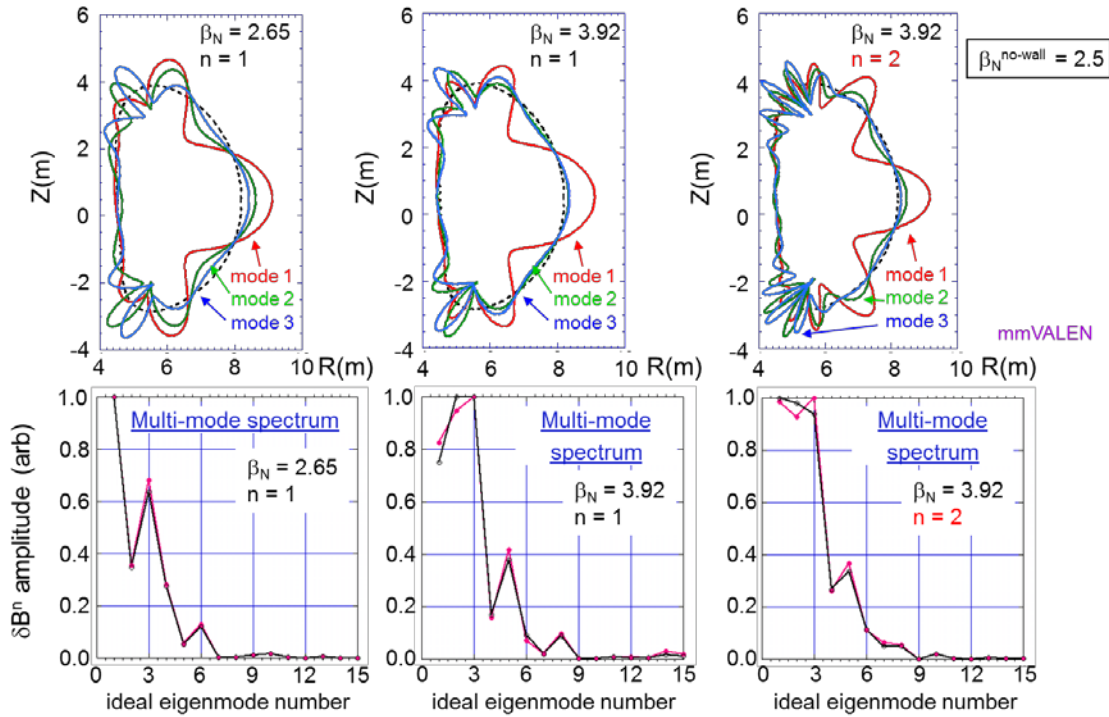


Figure 2.2.1.1.3: Multi-mode RWM analysis of ITER advanced scenario discharges, demonstrating a significant eigenmode spectrum in addition to the standard single ideal eigenmode typically assumed in control calculations.

profile can be explored and pushed for limits on plasma stability. This will be important for defining the operating regime of NSTX-U, setting boundaries to be avoided with control techniques, as well as setting up future experiments for assessing ways to improve stability at those boundaries.

2.2.1.1.3 Recover and test upgraded RWM multi-component sensor and model-based state space control with independent actuator coils, including $n > 1$ and multi-mode control

Computation of the multi-mode spectrum of ITER advanced scenarios (Figure 2.2.1.1.3) has shown that these plasmas exhibit a broader mode spectrum beyond the standard “single-mode” analysis that is typically conducted and that is used in tokamak mode control systems. Operation of NSTX-U plasmas in the high beta operational space accessible by the device will allow testing of the importance of this expanded mode spectrum to further improve active mode control.

In addition to the off-line multi-mode analysis capabilities used on NSTX, which is directly applicable to NSTX-U, the present model-based RWM state space control system initially used on NSTX (in plasmas that reached very high values of key stability parameters $\beta_N > 6.4$, $\beta_N / l_i > 13$), enables the use of the multi-mode spectrum in real-time global mode control. The new

NSTX-U capability of independent RWM coil actuator control combined with an expanded RWM state-space controller will allow multi-mode spectrum control enabling needed research to determine how varied details of the mode spectrum (including 3D mode effects), and 3D detail of the device conducting structure can improve disruption avoidance by improved mode control.

2.2.1.1.4 Study and attempt initial control of internal MHD modes during current ramp-up

Early MHD modes locking to the wall were a big source of low density disruptivity in NSTX. These modes were always associated with the rational surfaces entering the plasma. Modes at $q=2, 3,$ and 4 have been observed to lock, with a large degree of variability in the rotation damping dynamics. In NSTX, empirical changes to the fuelling were used to prevent modes from locking. Changes in global parameters due to fuelling changes were quite subtle, but changes to rotation dynamics were profound. A better understanding of mode amplitude and torque dynamics is needed. For example, are there small changes in resistive current evolution, or modification of the early EPs, and is there a measurable quantity to put under feedback control? These questions will be studied in NSTX-U to help improve reliable plasma start-up.

2.2.1.2 Year 2 of NSTX-U operation

2.2.1.2.1 Validate RWM physics at reduced v^* and varied fast ion populations

Future devices will have decreased collisionality compared to present devices, and previous RWM stability models predicted decreased v^* to be universally destabilizing. In contrast, in kinetic theory reduced ion-ion collisions have been shown to lead to a significant stability increase when the plasma rotation frequency is in a stabilizing resonance with the ion precession drift frequency [8]. When the plasma is in a reduced stability state with rotation in between resonances, collisionality was shown to have little effect on stability [8]. NSTX-U will have lower collisionality than NSTX, helping to test this physics.

Global modes are affected by the fast particle profile in high beta plasmas. Evidence of this has been reported in NSTX research, and continues to be an active area of research [9]. This is especially important for ITER, as a significant alpha particle fraction is expected to be required to stabilize ITER advanced scenario equilibria when utilizing the kinetic RWM stability theory tested on NSTX (Reference [8], Figure 5). The addition of three additional neutral beam heating sources on NSTX-U, all aimed at the plasma more tangentially than the present sources (farther from the magnetic axis), will allow a greater variation of the energetic particle profile to more fully quantify and verify its influence in the kinetic RWM stability model for further application to ITER and FNSF.

2.2.1.2.2 Utilize off-axis NBCD to vary V_ϕ and q-profile and investigate RWM/TM stability

A major new capability of NSTX-U beyond NSTX is the new neutral beam, which will inject off-axis. This capability can be used to drive current off-axis and therefore change the q-profile, which could have a major effect on the macroscopic stability of the plasma. Additionally, off-axis injection can potentially change the plasma rotation profile substantially, leading to a broader rotation profile. This too would have a major impact on stability, particularly RWM stability, and will be fully investigated and compared to theoretical predictions.

2.2.1.2.3 Understand and control internal MHD mode physics for long pulse, high performance scenarios

Coupled $m/n=1/1$ and $2/1$ modes limited many long-pulse scenarios in NSTX. A database of 138 MSE constrained equilibrium reconstructions showed that EPM and ELM triggers cause modes to onset at large values of q_{\min} , with rotation shear at $q=2$ likely playing a role. There were also “triggerless” modes, that were probably initiated by internal kink or infernal modes as q_{\min} approached 1. However, it was also possible to have discharges that sit with q_{\min} just above one for long periods. In NSTX-U, NBCD will be used to understand what the required increment of q_{\min} above rational values is to avoid internal/infernal modes.

2.2.1.3 Year 3 of NSTX-U operation

2.2.1.3.1 Utilize rotation control to improve RWM/TM stability

Strong, precise, and controllable neoclassical toroidal viscosity (NTV) effects were observed in NSTX. This allowed routine open-loop v_ϕ profile alteration, which is not routinely performed on other devices. NSTX-U will also provide plasma rotation control by novel means (e.g. using 3D fields to change plasma rotation in closed-loop feedback) and so allow more controlled studies of the impact of plasma rotation profile on plasma stability.

2.2.1.3.2 Explore the lowest v^* regimes and test RWM/TM stability

By the third year of operation of NSTX-U, the collisionality of the device in high performance scenarios will be significantly less than in NSTX. Studies of the effect of collisionality on stability will continue from the previous years (see Section 2.2.1.2.1). Operation at up to a factor of 4 lower collisionality, with an order of magnitude variation of this quantity, will experimentally substantiate present projections of RWM stability to lower collisionality based on kinetic RWM theory (Figure 2.2.1.3.2) [8].

2.2.1.3.3 Assess and optimize tradeoffs between V_ϕ , q-profile, β to improve RWM/TM/internal MHD mode stability

The rotation profile, q-profile and plasma beta are all affected by the neutral beams in a complex way. Therefore, a careful assessment of the interaction between the feedback control systems for V_ϕ , q-profile, and β will be necessary to optimize their interplay to produce positive results for plasma stability.

2.2.1.4 Year 4 of NSTX-U operation

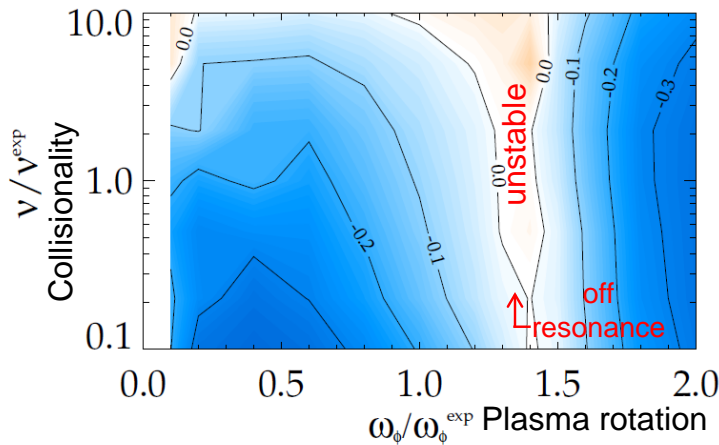


Figure 2.2.1.3.2: Computed effect of plasma collisionality on RWM stability (contours of normalized growth rate) as a function of plasma rotation, illustrating the effect of proximity to the ion-precession drift resonance.

2.2.1.4.1 Utilize non-axisymmetric control coil (NCC) to control V_ϕ -profile and improve RWM/TM stability

The installation of the NCC will allow studies of NTV physics, and v_ϕ control with $n \leq 6$. Building off of previous year’s research (see Section 2.2.1.3.1), unfavorable rotation profiles can be avoided, and favorable profiles maintained with this capability. A particularly exciting aspect of this research is the possibility of increasing

v_ϕ via $n > 1$ toroidal propagation with the NCC.

2.2.1.4.2 Investigate the combination of V_ϕ -profile, β -feedback, and active mode control to improve RWM/TM/internal MHD mode stability and to sustain high performance plasmas

Building upon the experiences of previous years operation (see Section 2.2.1.3.3), by the fourth year of NSTX-U operation, a good working understanding of the various feedback and control mechanisms should allow all of them to be used in concert to sustain high performance discharges. Rotation and beta feedback will be used to avoid unfavorable plasma conditions for stability, while advanced active feedback systems will be used to control the plasma in the case of excursions from optimal operating regimes.

2.2.1.4.3 Extend the study of RWM multi-mode control with various NCC coil combinations

The NCC can provide quantitative evaluation of the importance of multi-mode spectrum (n and m) for RWM control and dynamic error field control. The RWM state-space controller allows far greater flexibility of global mode stabilization physics studies with these coils, with a relatively simple control software upgrade. The spectrum will gain helicity with the NCC, which is important to expand research. An $n > 1$ mode spectrum has been observed in NSTX, but the importance of $n > 1$ control or dynamic correction has never been tested. Additionally, the physics and control of “nonrigid” mode evolution can be studied, as well as RWM state space control with an ITER-similar coil set.

2.2.1.4.4 Provide FNSF/Pilot projection on macroscopic stability

Four years of operation with NSTX-U will culminate in the ability to make projections to next step ST devices, such as FNSF, in the area of macroscopic stability. Specifically, RWM stability as a function of collisionality, rotation, and energetic particle profiles will have been explored and compared to theoretical projections, and experience with advanced active feedback systems operating at the same time as various other control systems (rotation, beta...) will inform schemes for next step devices.

2.2.2 Thrust 2 – Understand 3D field effects and provide physics basis for optimizing stability through equilibrium profile control by 3D fields

2.2.2.1 Error field correction and control to stabilize locking and tearing modes

2.2.2.1.1 Identify $n > 1$ intrinsic error fields and optimize correction using independent actuator coils

NSTX-U will have significant modification in some of machine components such as the center-stack and NBI beam ports, and may have different intrinsic error fields. NSTX had two main components of intrinsic errors: (1) $n=1$ by OH-TF joint distortion and (2) $n=3$ by PF5 non-circularity [10]. The same PF5 coils will be used for NSTX-U and will contain the same error fields, although the coupling to the plasma and thus the optimal correction will be different. The OH-TF joint error is not expected to be as substantial as NSTX, but nevertheless will be investigated as mechanical forces on the center-stack are intrinsic to ST devices. This part will require a fair amount of effort and time in the first-year NSTX-U operation, since the identification and correction of intrinsic error fields is critical for studies of 3D field physics and generally for better performance.

The plan is first to charge the OH, TF, PF coils independently and to measure the vacuum field using magnetic sensors to see the relevance of the previous error field model in NSTX. The model will be revised if necessary. Then we will perform an $n=1$ compass scan, by ramping up error field correction (EFC) coil currents, to see if the locking response is non-axisymmetric. The $n=2$ compass scan will also be done by utilizing 6 independent switching power amplifiers (SPAs). It is not possible to rotate $n=3$ fields before the new non-axisymmetric control coil (NCC) is installed, but the optimal $n=3$ correction that was used to maximize the total toroidal angular momentum, as shown in Figure 2.2.2.1.1, will be tested again. After each investigation for each $n=1-3$, we will optimize the static $n=1-3$ error field correction and utilize it if necessary to improve plasma performance.

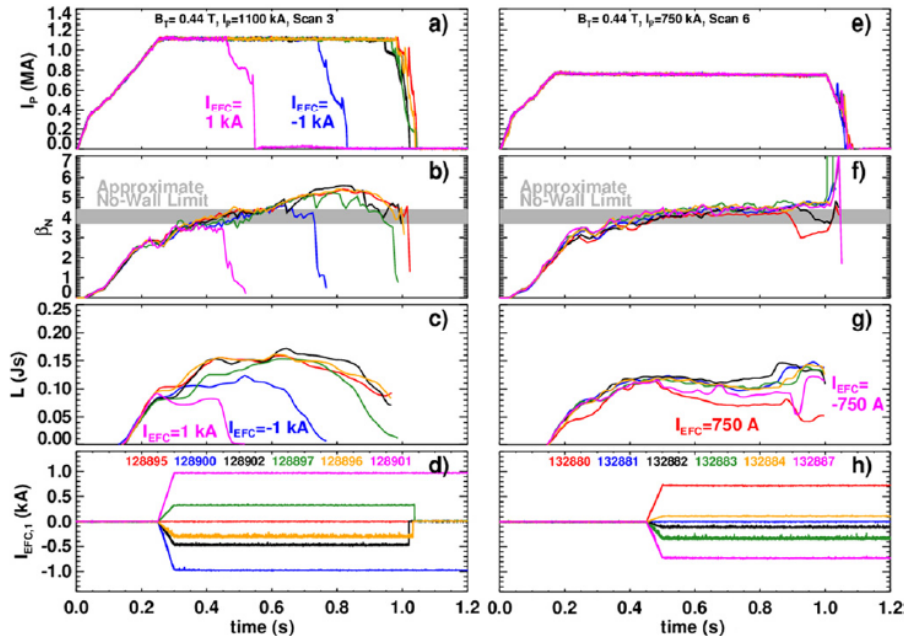


Figure 2.2.2.1.1: $n=3$ magnetic braking in NSTX, showing the optimal correction in yellow (d) and green (h) that maximized toroidal angular momentum in (c) and (g).

2.2.2.1.2 Explore upgraded 3D capabilities of active mode control and dynamic error field correction

Active mode control and dynamic error field correction are also important especially for high- β since various MHD modes, including the RWM, can easily arise in such a high-performance operation. Also the OH-TF error field was time-dependent and the correction became more uncertain in high- β due to strong interaction with the plasma. The $n=1$ active and dynamic control algorithms were highly successful in NSTX as shown in Figure 2.2.2.1.2, and so the plan for the first year is to restore and explore the $n=1$ capability in NSTX with the 6 independent SPAs.

2.2.2.1.3 Optimize and combine dynamic error field correction with intrinsic error field correction

The 6 independent SPAs will make any $n=1-3$ combination of static and dynamic error field correction possible during operation. Based on the exploratory study for the $n=1$ dynamic error field correction in the first year, the optimization of the algorithm will be studied at the interim between experimental campaigns and will be tested in the second year.

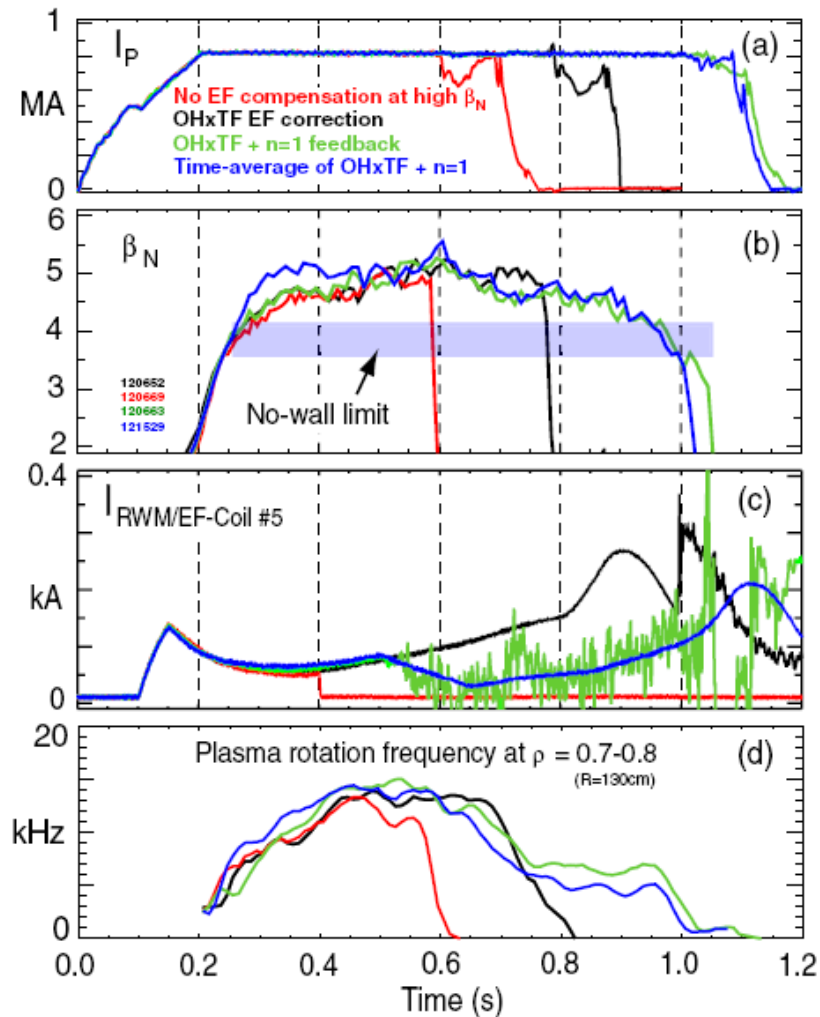


Figure 2.2.2.1.2: Various successful error field correction, including the dynamic error field correction in green, which sustained plasma above the no-wall limit and substantial toroidal rotation.

The optimized n=1 dynamic correction will be first compared with the pre-programmed n=1 error field correction. Next the combination of the dynamic and static correction will be tested with different weighting factors and possibly optimized for the best n=1 error field correction. The n>1 dynamic correction will be challenging due to weak plasma response and weak coupling between plasma and magnetic sensors. However, NSTX studies show that n=2-3 RWMs can be significantly detected, and so the possibility for n>1 dynamic correction will be tested (time permitting) by applying the n=2 or n=3 EFC currents to see if the correction algorithm can detect and actuate the proper responses back.

2.2.2.1.4 Initiate the investigation of non-resonant vs. resonant error field effects

The study of the intrinsic error field has been focused on the resonant component and its compensation to avoid locking. However, recent studies with both resonant and non-resonant field applications show that the resonant error field threshold can be significantly altered by non-resonant error fields. Figure 2.2.2.3.1 shows the comparison between the resonant field vs. locking scaling including rotation in NSTX high- β locking experiments. Here the $n=1$ resonant field thresholds are significantly low in the blue cases, due to the additionally applied $n=3$ fields that decrease the rotation.

The importance of the non-resonant error field correction is clearly demonstrated by recent proxy experiments in DIII-D. In these experiments, the error field was created by external C-coils, and the correction was added with I-coils. The I-coil correction is optimized with conventional compass scans and this optimization is expected to remove the resonant error field irrespective of the error field sources. However, the optimization for the proxy C-coil error field was not as successful as the intrinsic error field, which may be due to much larger non-resonant components remaining after the correction. Indeed, IPEC and NTV analysis showed the NTV is increased even more than the linear sum of NTV by each C-coil and I-coil field, while the resonant field is greatly reduced, as shown in Figure 2.2.2.3.1-2. However, although the NTV analysis for the proxy cases shows the possible resolution may be found in NTV, it is still not clear if the non-resonant component directly influences locking, or indirectly through the NTV rotational damping.

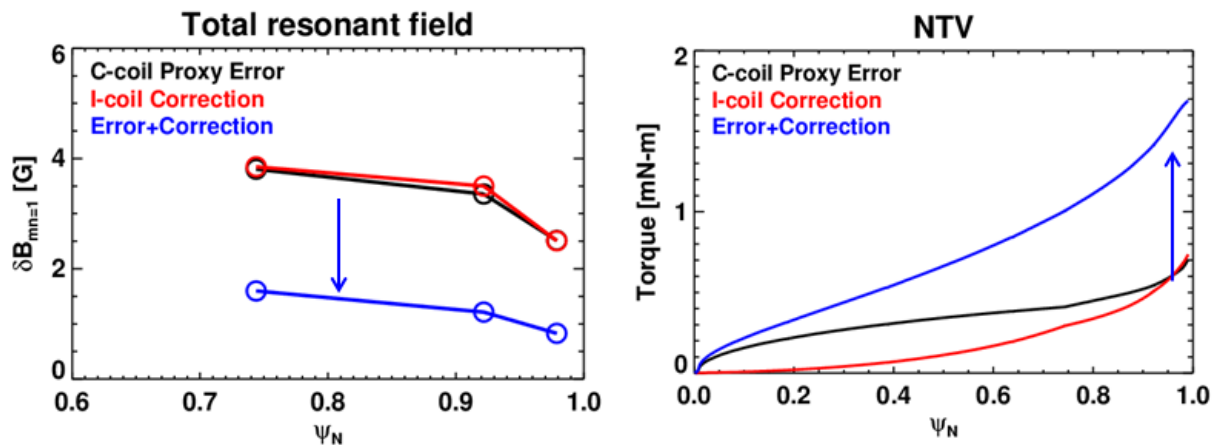


Figure 2.2.2.3.1-2: Total resonant field and NTV in proxy error field experiments in DIII-D. One can see C-coil + I-coil correction reduced the total resonant field, but substantially increased NTV.

NSTX-U will give a very good environment to study these non-resonant error field effects, especially when the NCC is equipped, but even before then by utilizing the 6 independent SPAs. We will investigate the $n=1$ locking threshold by changing $n>1$ non-resonant error fields. The goal is to see if the resonant locking threshold can be modified differently when similar rotation braking is added but with different non-resonant fields using $n=2$ and $n=3$ separately.

2.2.2.1.5 Utilize NCC and understand non-resonant and resonant error field effects vs. V_ϕ

The non-axisymmetric control coil (NCC), if installed, will enable fully systematic investigations of non-resonant and resonant error field effects with respect to the rotation. First the NCC will be utilized for $n=1$ error field correction with 12 different poloidal spectra, against the proxy error field created by the present RWMEF $n=1$ field. Figure 2.5.2.3 in NCC section shows that the resonant field created by 1kAt of the present RWMEF can be compensated by 0.5~3kAt from the NCC coils depending on the poloidal phase shift between the upper and lower set of coils. That is, the 12 different NCCs can be used to completely remove the resonant field, but to provide different non-resonant field spectrum as well as the rotation profile.

Then plasma responses, such as locking thresholds, will be studied as a function of non-resonant field spectrum and separately as a function of the toroidal rotation. The study can be extended by making attempts to produce a similar toroidal rotation profile using different toroidal harmonic perturbations, such as $n=2$ or $n=3$. This will enable us to better conclude if the non-resonant error field influences the resonant braking directly by its own mechanism or indirectly by toroidal rotation modification.

2.2.2.1.6 Timescale for research in the area of error field correction and control to stabilize locking and tearing modes

Year 1:

- Identify $n > 1$ intrinsic error fields and optimize correction using independent actuator coils.

Year 2:

- Explore upgraded 3D capabilities of active mode control and dynamic error field correction.
- Optimize and combine dynamic error field correction with intrinsic error field correction.

Year 3:

- Initiate the investigation of non-resonant vs. resonant error field effects.

Year 4:

- Utilize NCC and understand non-resonant and resonant error field effects vs. V_ϕ .

Year 5:

- (Add text here)

2.2.2.2 Understanding neoclassical toroidal viscosity (NTV) physics to control (rotation) braking

2.2.2.2.1 Initiate NTV physics investigation with enhanced 3D field spectra and NBI torque profile

NSTX-U will have larger flexibility to change the toroidal torque and rotation, since the 6 independent SPAs will allow the application and switching of $n=1-3$ fields, and also the 2nd off-axis NBI system will produce various different profiles of injection torques. In order to find the effects of the second NBI system, we will use the standard $n=2$ and $n=3$ field application to cause NTV torque, but with different NBI injection methods.

2.2.2.2.2 Investigate NTV physics at increased pulse lengths and behavior at reduced v^* regime

In the second year, the focus of NTV physics studies will be shifted to parametric dependencies, especially on the collisionality. For this, a couple of standard combinations between the $n=3$ (or $n=2$) applied field and NBI configurations will be selected, and will be tested with different powers and levels of density. Generally an increase of NTV torque is expected, unless the rotation is far off the rotational resonances. Figure 2.2.2.2 shows the analytic $n=1$ and $n=3$ NTV estimations as a function of rotation and collisionality, based on the field calculations by IPEC and the transport calculations by combined NTV theory. One can see that NTV increases when the collisionality decreases through the rotational resonances, such as superbanana-plateau

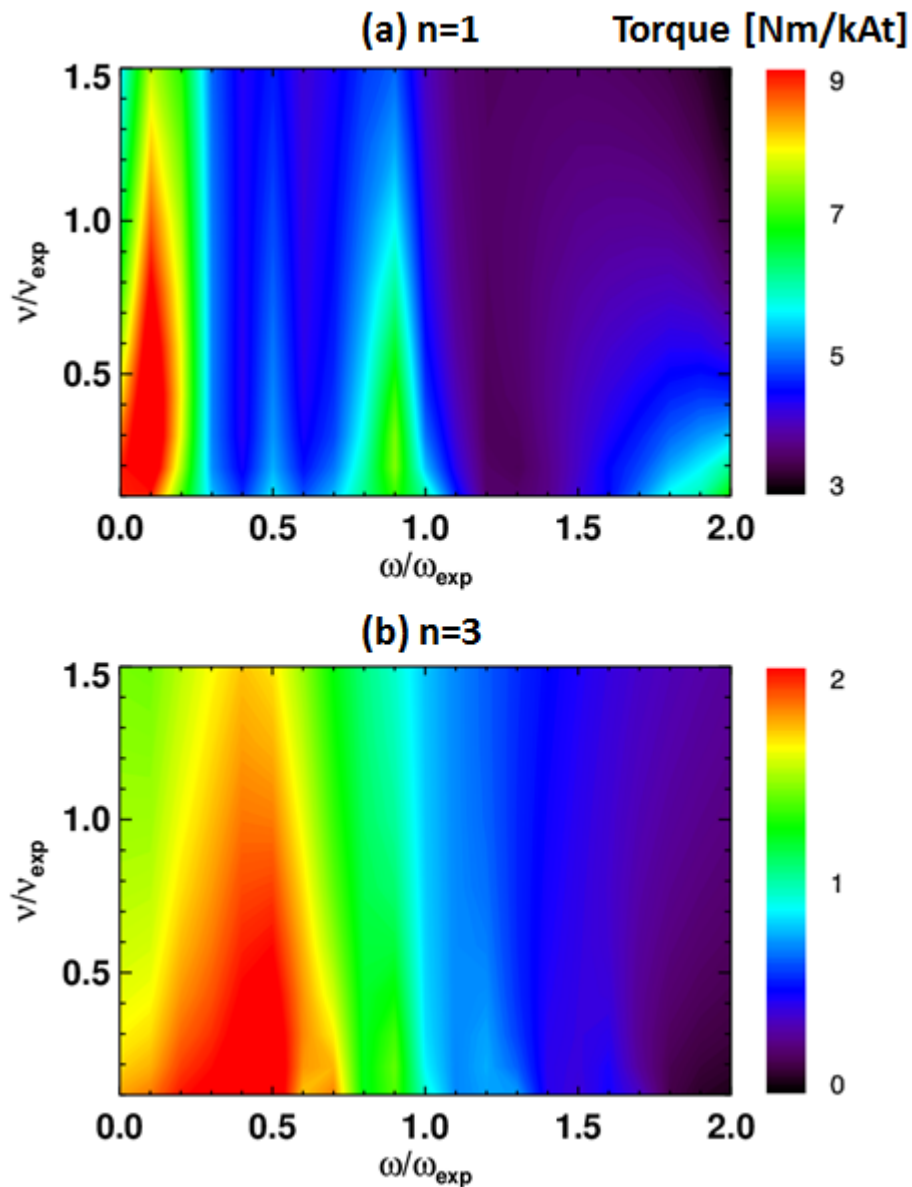


Figure 2.2.2.2.2: Analytic NTV calculations for (a) $n=1$ and (b) $n=3$ magnetic braking in NSTX, as a function of the collisionality and rotation.

(SBP) or bounce-harmonic (BH) resonances. So the plan is to validate this prediction and to compare and understand NTV physics in reduced collisionality.

2.2.2.2.3 Investigate NTV physics vs. V_ϕ and q-profile with new NBIs and independent actuator coils

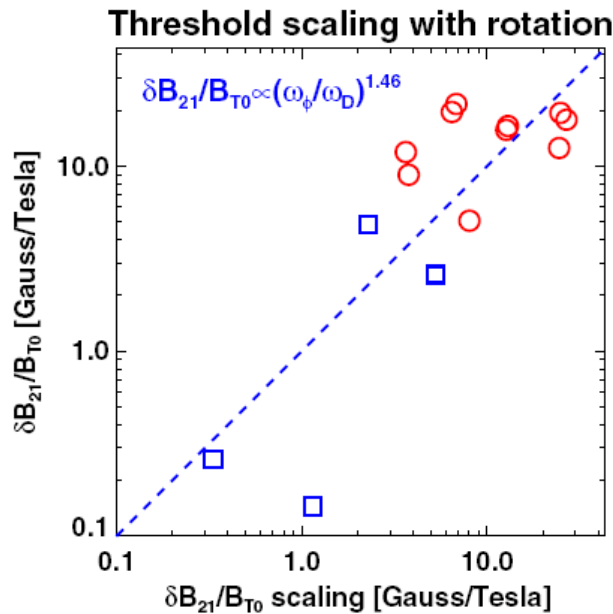


Figure 2.2.2.3.1: Comparison between the resonant field (Y) vs. resonant field scaling. Rotation scaling is additionally required for blue points, which included $n=3$ rotation braking.

Another important parameter for NTV is the rotation itself, as already illustrated by Figure 2.2.2.2.2. Interestingly, the $n=1$ and $n=3$ trends are very different, as one can see the clear separation between rotational resonances only for $n=1$. This is due to narrower gaps by $1/n$ between SBP and BH resonances at higher n . This also implies very different selectivity of the $n=1$ and $n=3$ NTV torque. That is, the $n=1$ field can be a very stable actuator to produce off-resonant rotation, but the $n=3$ field can be more flexible on any level of rotation while it can be easily unstable in very low rotation due to the acceleration of the toroidal torque. These two different natures of NTV physics as a function of rotation will be tested with modulated NBI power and new SPAs.

The q-profile is not directly linked to NTV physics, but it can alter the non-axisymmetric variation in the field strength through the plasma response and can result in a strongly modified NTV torque profile. The q-profile will be varied primarily by different combination of NBCDs. Since NBCDs will also affect the rotation profile, the rotation and q-profile effects on NTV will be studied together.

2.2.2.2.4 Study NTV physics in the lowest v^* regimes

We will extend the study of NTV dependency on the collisionality by achieving the lowest density and collisionality regime, which will be directly relevant to future ST applications. The prediction of the analytic theory is a large increase of NTV through the rotational resonances. However, verification work with the global code FORTEC-3D shows that even the analytic NTV may be underestimating the effects of non-resonant field components, as illustrated in Figure

2.2.2.3.2. Therefore, the NTV validation in the lowest collisionality regimes will be especially important to resolve the different predictions between the numerical and analytic computations.

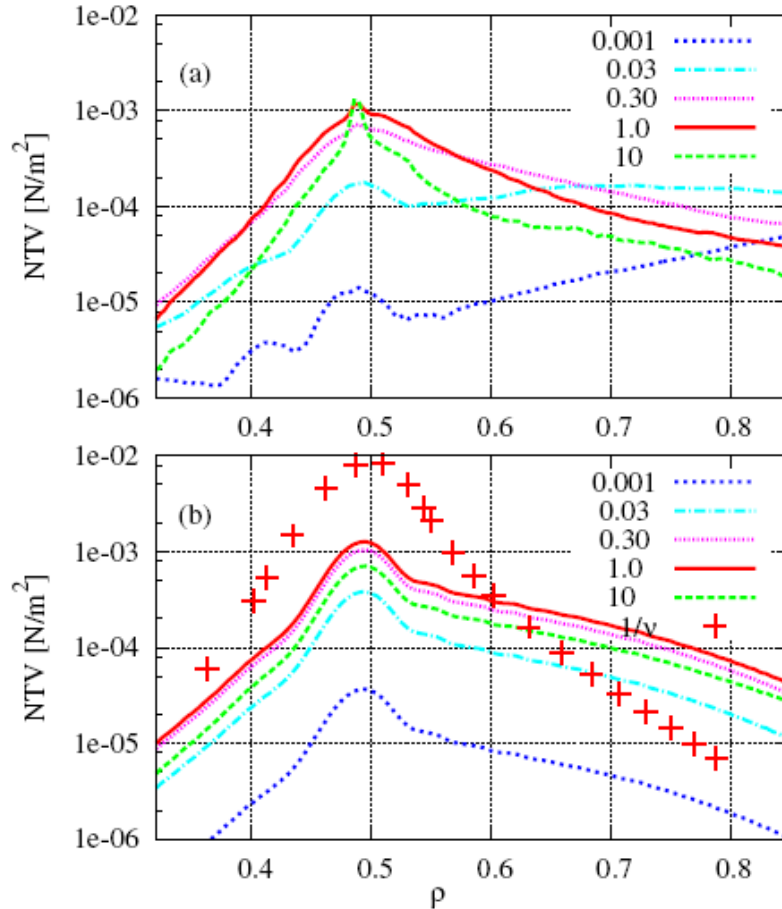


Figure 2.2.2.3.2: Comparison between FORTEC-3D (Upper) and analytic NTV (Lower) for different collisionality. One can see good agreements in general, but also a substantial discrepancy in the lowest collisionality.

Also in a practical point of view, rotation braking itself, rather than NTV braking, should be investigated. The subtle difference can increase uncertainty in a very collisional regime since the injection torque by NBIs and also the intrinsic torque can arise differently. For instance, the high temperature in the lowest collisionality can increase the intrinsic torque linearly, and so even if the NTV braking torque increases, the rotation braking can be practically similar. This part of the study will provide the experience necessary for rotation control in NSTX-U.

2.2.2.2.5 Optimize V_ϕ feedback control in regimes of high non-inductive fraction to improve RWM/TM stability

In Year 3, we will begin a systematic study of rotation control. A real-time toroidal velocity (RTV) measurement system has been successfully tested in NSTX (Figure 2.2.2.3.3) and will be utilized for rotation feedback control in NSTX. The neutral beams will be used as actuators, to control the input torque and rotation. In this first step, the goal is to explore the roughly

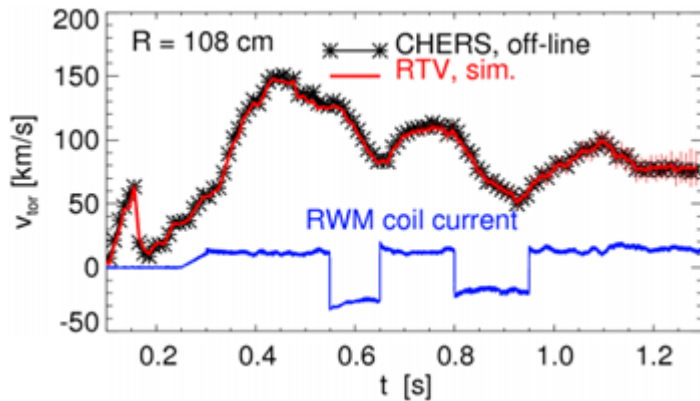


Figure 2.2.2.3.3: Successful algorithm test of real-time toroidal velocity measurement in NSTX.

accessible level of rotation at the center and in the pedestal region using NBI.

Within the accessible level of the rotation, the rotation feedback system with RTV and NBIs will be tested to improve RWM/TM stability. We will set a few combinations of the core and edge rotations that have different RWM and/or TM stability characteristics, and will test if the feedback system can maintain the rotation.

2.2.2.2.6 Utilize 3D fields to assess and optimize tradeoffs between V_ϕ , q-profile, β to improve RWM/TM/internal MHD mode stability

Neutral beams can modify the input torque and rotation, but can also significantly change the q-profile by driving plasma current and β by plasma heating. The 3D field is the essential actuator for the rotation control system in this regard, as a 3D field can change nothing but the rotation when it is sufficiently non-resonant. We will begin with $n=3$ fields, which can be applied on the top of the $n=1\sim 3$ intrinsic error field correction using the 6 independent SPAs.

The goal in this step is to investigate the accessible level of the rotation in the same q-profile and β , by utilizing both NBIs and 3D fields. In particular, the q-profiles and β values favorable to RWM, TM, and internal MHD mode stability will be selected and maintained while the rotation is changed. Next we will investigate the variation of the q-profiles or β values while the rotation is maintained and optimize tradeoffs to improve each MHD stability condition.

2.2.2.2.7 Examine FNSF/Pilot projections on 3D field physics understanding

(Add text here)

2.2.2.2.8 Timescale for research in the area of understanding neoclassical toroidal viscosity (NTV) physics to control (rotation) braking

Year 1:

- Initiate NTV physics investigation with enhanced 3D field spectra and NBI torque profile.

Year 2:

- Investigate NTV physics at increased pulse lengths and behavior at reduced v^* regime.
- Investigate NTV physics vs. $V\phi$ and q -profile with new NBIs and independent actuator coils.

Year 3:

- Study NTV physics in the lowest v^* regimes.
- Optimize $V\phi$ feedback control in regimes of high non-inductive fraction to improve RWM/TM stability.

Year 4:

- Utilize 3D fields to assess and optimize tradeoffs between $V\phi$, q -profile, β to improve RWM/TM/internal MHD mode stability.

Year 5:

- Examine FNSF/Pilot projections on 3D field physics understanding.

2.2.3 Thrust 3 – Understand disruption dynamics and develop techniques for disruption avoidance and mitigation in high-performance ST plasmas

A key issue for ITER, and the tokamak/ST line of fusion devices in general, is the avoidance and mitigation of disruptions. As a general goal, disruptions must be avoided. The research program in Thrusts 1 & 2 of this chapter, as well as in Thrusts 2 & 3 of the ASC chapter, develops many of the necessary tools for disruption avoidance. These tools by themselves, however, are not sufficient to meet the stringent requirements for reliable tokamak/ST operations. The present thrust describes three additional research tasks for disruption avoidance, mitigation, and characterization.

The first sub-thrust, described in Section 2.2.3.1, describes the development of techniques for integrated disruption avoidance. Methods developed in this Section combine seemingly disparate

actuators and measurements, in order develop a more integrated control of global stability. For instance, resonant field amplification methods will be developed to assess global stability, and may be coupled to the β_N or rotation control algorithms ensure that the plasma remains in a stable regime. Similarly, the state-space RWM control... (Add text here)

The second sub-thrust, described in Section 2.2.3.2, addresses the topic traditionally known as disruption “mitigation”. This topic is of great importance to ITER, where methods to terminate a discharge without excessive thermal or mechanical loading of the plant are required. This research will focus on two technologies for rapidly terminating a tokamak discharge. Massive gas injection (MGI) will be explored: the poloidal angle dependence of mitigation efficacy will be examined, and modeling of the gas penetration with DEGAS-2 will be done. A novel electromagnetic particle injector (EPI) will be developed. This technology has the potential to very rapidly deliver large amounts of the material to the plasma, and will be tested on NSTX-U. Note that this topic is complementary to that discussed in ASC Thrust 3, focusing on rapid discharge terminations using traditional inductive ramp-down techniques. NSTX-U is also capable of studying runaway current suppression as described in Section x.

The final sub-thrust, described in Section 2.2.3.3, focuses on the physics of disruptions themselves. Key topics to be addressed here are physics of, and heating loading from, the thermal quench of a disruption, and generation of halo currents.

2.2.3.1 Integrated disruption avoidance

Many other sub-Sections of this plan discuss elements of disruption avoidance. For instance, the heating power can be modulated to achieve a desired value of β_N . NTV and beam torques can be used to target specific rotation profiles. RWM control, based on a state-space or PID formulation, can be used to apply $n \geq 1$ magnetic fields in response to measured magnetic perturbation. Each of these control schemes uses the natural combination of measurement and actuator, in an essentially stand-alone manner.

However, disruption avoidance will likely require that seemingly disparate measurements and actuators be combined; the development of two such schemes is the purpose of this Section 2.2.3.1. The first method relies on realtime assessments of “resonant field amplification” (RFA) to provide stable targets for the rotation profile and β_N . The second method uses the state-space controller to provide similar control targets.

2.2.3.1.1 Realtime RFA measurements for the control of β_N and rotation

(Add text here)

2.2.3.1.2 Use of the RWM state-space machinery for the control of β_N and rotation

(Add text here)

2.2.3.1.3 Timescale for research in the integrated disruption avoidance area

Year 1:

Year 2:

Year 3:

Year 4:

Year 5:

- Integrate MS control to avoid RWM/TM/ELM/internal MHD instability and disruption, with disruption mitigation protection.

2.2.3.2 Rapid shutdown techniques via mass injection for disruption avoidance

As noted in the introduction to this thrust, a fast discharge termination method is needed to minimize the deleterious effects of the disruption, particularly the large heat loading from the

thermal quench and the generation of large populations of runaway electrons. Massive Gas Injection (MGI) is one approach to addressing this difficult issue for ITER. Research in NSTX-U will compare MGI from different poloidal locations to assess the gas penetration efficiency from each of these locations. We are starting to model gas penetration using DEGAS-2 to quantify the gas penetration past the SOL for NSTX-U. For disruptions in ITER that have short warning times of less than 10ms, the MGI system may not perform satisfactorily. For these extreme cases, for which the ITER disruption mitigation system (DMS) must be designed, we are developing a fast impurity injection system called the Electromagnetic Particle Injector

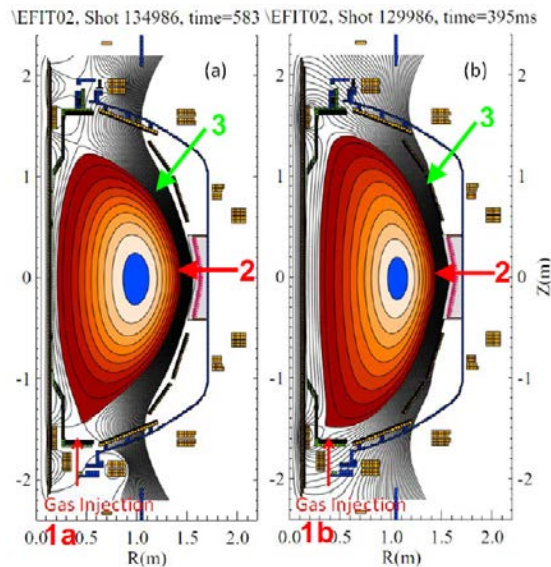


Figure 2.2.3.2.1: Shown are the planned Massive Gas Injection locations on NSTX-U. (1a) Private flux region, (2) mid-plane injection, (1b) high field lower SOL region and (3) outer SOL above the mid-plane.

(EPI). These planned activities for NSTX-U are briefly described in Sections 2.2.3.2.1 through 2.2.3.2.3.

Note that realtime disruption detection methods are described in Section 9.2.4.X.X of the ASC chapter. Those methods will be used to trigger these mitigation technologies in NSTX-U to test realtime disruption mitigation. Also, the diagnostics required for these studies will be described in the disruption physics sub-thrust, in Section 2.2.3.X.X.

2.2.3.2.1 Massive gas injection experimental development

At present, massive gas injection (MGI) appears to be the most promising method for safely terminating most discharges in ITER [11,12,13,14,15]. MGI involves the rapid injection of large quantities of gas into the tokamak discharge; the quantity of gas is typically several times the inventory of the plasma discharge. Usually some fraction of the injected gas has a high-Z component such as argon or neon. Requirements for the mitigation of disruption effects fall into

three categories: (1) Reducing thermal loads on the first wall and the divertor; (2) reducing electromagnetic forces associated with “halo” currents, i.e. currents flowing on open field lines in the plasma scrape-off layer; and (3) suppressing runaway electron (RE) conversion during the current quench phase of the disruption. To accomplish these in ITER, it is projected that about $500 \text{ kPa}\cdot\text{m}^3$ of helium with some noble gas fraction will be required.

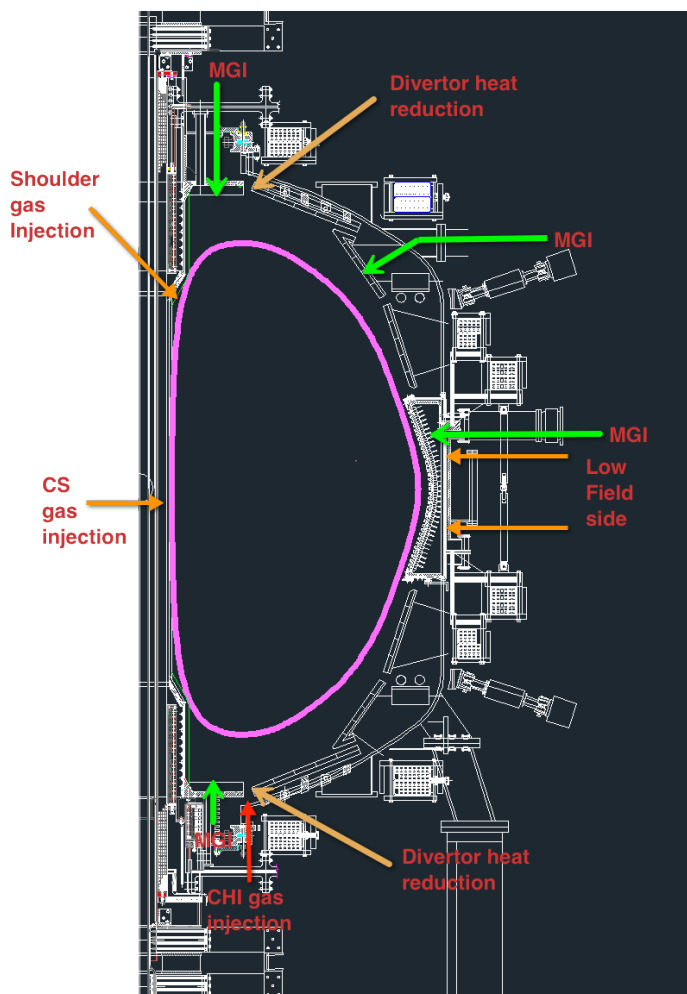


Figure 2.2.3.2.1-2: MGI gas injection locations on NSTX-U are shown by the green arrows.

has been cooled by a MGI pulse, needs to reach the $q=2$ surface for the onset of rapid core cooling to occur. On ITER, it is not known if a simple MGI pulse from multiple locations would be adequate because of its larger minor radius, the increased transit times for the neutral gas, and the larger expected scrape-off-layer (SOL) flows. Insight into ways for reducing the total amount of injected gas and optimizing the injection locations would further help with the design of a suitable system for ITER.

NSTX-U can offer new insight by injecting gas into the private flux and lower x-point regions of divertor discharges to determine if this is a more desirable location for massive gas injection. Injection from this new location has two advantages. First, gas injected directly into the private flux region does not need to penetrate the scrape-off-layer. Second, because the injection location is nearer the high-field side in standard D-shaped cross-sections, the injected gas should be more rapidly transported to the interior as known from high-field side pellet injection [16] and from high-field side gas injection work on NSTX [17]. By comparing massive gas injection from this new location to injection of a similar amount of gas from the outer mid-plane, NSTX-U can improve the knowledge of disruption mitigation physics and thus improve the DMS design for ITER.

To put the gas penetration issue in perspective, the private flux region in ITER is predicted to have an electron temperature of less than 2eV and an electron density below $2 \times 10^{20} \text{ m}^{-3}$ [18]. Representative values for these two parameters for detached DIII-D plasmas are an electron temperature of less than 1eV and electron density less than $5 \times 10^{19} \text{ m}^{-3}$ [19]. The relatively low electron temperature in the private flux region in both ITER and DIII-D is due to active gas puffing in the divertor region to obtain a detached divertor configuration, which is necessary to reduce divertor heat loads. The electron temperature and electron density in the SOL at the mid-plane region of ITER is predicted to be about 100eV and $2 \times 10^{19} \text{ m}^{-3}$ [20]. The corresponding values for DIII-D are an electron temperature less than 20eV and an electron density less than $3 \times 10^{18} \text{ m}^{-3}$ [21]. The parameters for the NSTX-U could be expected to be similar to those for DIII-D.

These numbers show that plasma parameters in the SOL region for present large tokamaks as well as the projected SOL parameters for ITER are much more challenging for neutral gas penetration compared to the parameters in the private flux region. This is the motivation for proposed experimental work on NSTX-U. These parameters will be used as input in DEGAS-2 simulations to theoretically assess the gas penetration efficiency as a function of SOL and private flux region parameters and will eventually be compared to experimental observations from NSTX-U.

The primary goal of the MGI experiments in NSTX-U is to compare the gas penetration efficiency as gas is injected from the different poloidal locations shown in Figure 2.2.3.2.1. These are (1a) the private flux region, (2) the mid-plane region, (1b) high-field side outer SOL region, high-field side inner SOL region and (3) outer SOL region above the mid-plane. A second objective is knowing the uniformity of the radiated power profile. The third objective is to assess the reduction in divertor heat loads and halo currents. The importance of the $q=2$ surface proximity to the plasma edge will be studied by gas injection at different times during the discharge as the $q=2$ surface evolves. The eventual goal of these studies would be to design a system for NSTX-U that could automatically trigger the MGI system based on input received from sensor provided data on an impending disruption. For these up-coming experiments on NSTX-U we have assigned four ports for MGI. The green arrows in Figure 2.2.3.2.1-2 show these MGI port locations.

The gas assimilation efficiency will be measured by obtaining closely spaced (in time) Thomson scattering density profiles just prior to and after the MGI gas begins to interact with the edge plasma but before the thermal quench phase has initiated. EFIT reconstructions would provide the plasma shape and volume. H-alpha detectors would be used to establish the time of contact of the MGI gas with the edge plasma. The time delay between this and the time when the individual MGI valve is triggered would provide the overall system response time for each gas injector. Starting from the time when the MGI gas first makes contact with the edge plasma, the Thomson scattering system would be triggered (at 0.5, 1, 1.5ms) to obtain density profiles before the plasma shape begins to significantly distort or the before the Thomson scattering system detectors saturate. **[Need to find out when they will saturate]**. Since the Thomson scattering system measures local density this is preferred over the NSTX-U multichord interferometer system as it avoids the issue of profiles obtained using Abel inversion from a few interferometer chords. However, depending on the amount of injected and assimilated gas both systems will be needed to obtain reasonable estimates for the amount of gas assimilated by the plasma discharge. Measuring this parameter has been challenging in other tokamak and will prove to be challenging on NSTX-U as well as these diagnostics are not designed for the very high density plasmas that result from assimilation of large quantities of gas.

A concern with localized gas injection for ITER is that the radiation profile could be toroidally localized to a region near the gas injection port. Depending on the plasma parameters, this could lead to localized heat deposition on nearby walls leading to localized melting. Thus measurement of the radiated power profile at three or more toroidal locations is important. This is discussed in detail in a subsequent Section, including the need for a new-dedicated diagnostic. Here we note that the NSTX-U multi-chord bolometer array and the multi-chord Soft X-ray arrays will be used to obtain the radiated power and soft X-ray emission profiles using an Abel inversion method from a dense array of chords.

The spatial distribution of the divertor heat loads will be measured with two color divertor fast infrared cameras. These were successfully used during the FY10 NSTX run campaign to measure divertor plate temperatures during the Snowflake divertor experiments. These will be complemented with eroding thermocouples that would provide an independent measurement of the divertor plate radial temperature profile at a few [how many?] toroidal locations. Halo current sensors on the divertor plates [toroidal location and number?] will provide data on the extent of halo currents during the different disruption mitigation scenarios and during unmitigated disruptions.

We will provide NSTX-U MGI results to groups using NIMROD, KPRAD, and the EIRENE-SOLPS codes to simulate NSTX-U experimental observations.

2.2.3.2.2 MGI simulations using the DEGAS-2 code

In support of Massive Gas Injection (MGI) studies on NSTX-U, we are conducting DEGAS-2 simulations [22,23] to better characterize the gas penetration physics and to improve the design of the MGI gas delivery system on NSTX-U.

There are two requirements for successful implementation of MGI in ITER. The first requirement is that an adequate amount of injected gas penetrates past the separatrix. This is related to the physics of neutral gas penetration through an energetic edge plasma region and the SOL. The ratio of the injected gas that couples to the tokamak discharge to the total amount of injected gas is referred to as the gas assimilation or gas penetration efficiency. The second part involves the physics of how the gas that penetrates past the separatrix distributes within the plasma discharge. The dynamics of the gas mixing is responsible for the resulting thermal quench timescales and radiated power profiles. This is referred to as gas dissipation physics inside the separatrix. While much work is in progress to understand the gas dissipation physics, for example through the use of the NIMROD code [24] the more fundamental gas penetration issue is poorly understood.

A review of the literature [11-14] shows that the amount of gas injected in MGI experiments in present tokamaks varies from 100 Pa.m³ to over 2000 Pa.m³, considerably less than the projections for ITER. The fraction of this gas that penetrates past the separatrix also varies widely, with penetration efficiencies of over 20% being reported for cases that have a short MGI pulse. To better quantify the amount of gas required in a MGI pulse we have initiated a DEGAS-2 Monte-Carlo code simulation effort to understand the extent of gas penetration through the SOL region and private flux regions. In addition to supporting NSTX-U needs, this simulation effort focuses on studying the fundamental issues of edge penetration to the separatrix, which is needed for predicting gas penetration efficiencies in ITER. This work complements other 3-D

MHD modeling (such as with the NIMROD code), initiated by the ITER organization, of the gas dissipation physics inside the separatrix.

Full DEGAS-2 model: For a full detailed simulation of the involved gas penetration physics, both the DEGAS-2 and UEDGE codes are required. The simulations would start with plasma parameters from a suitable NSTX-U discharge with neutral beam heating. The computational mesh needed for DEGAS-2 to model the region outside the separatrix region would be generated by the UEDGE code [25,26,27]. At the midplane, the total mesh width would be specified. This would typically be about 6cm for our cases. The outer edge of the mesh would be 8cm from the vessel wall, which would also be the location for the mid-plane gas injection location. The separatrix would be located 10cm from the gas puff location. Outside the UEDGE mesh, between that mesh and the vessel wall, there would be a coarser DEGAS-2 mesh. Here, DEGAS-2 subroutines would break the background region into a series of small interlocking triangles. Within each of these triangular “zones”, all parameters (source rates, densities, temperatures, etc.) would be held constant. Thus the SOL width would be about 2cm. Plasma temperature, density and SOL flows would be specified in the SOL region, the width of which could be changed to simulate varying plasma conditions. Gas would be injected from a small region, typical of the cross Sections of the MGI gas injection port, which would vary between 2-3 cm in diameter.

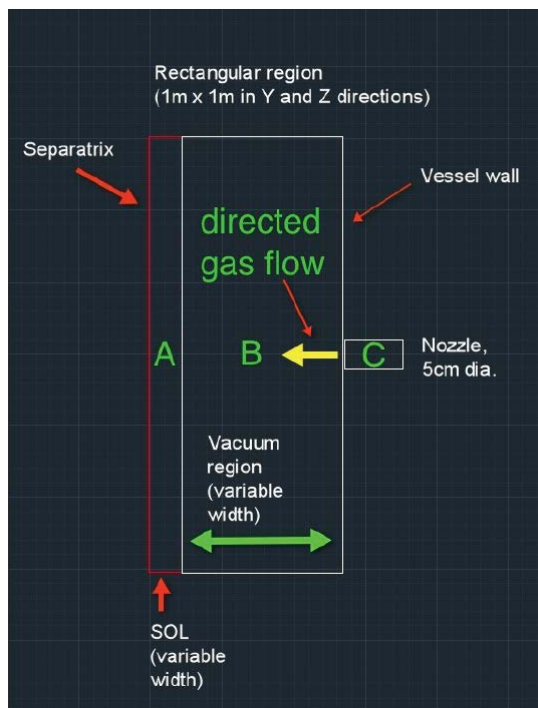


Figure 2.2.3.2.2: Simplified rectangular 3-D mode for DEGAS-2 simulations

As the molecules penetrate the plasma, they would undergo ionization, dissociation, and elastic scattering; resulting molecular ions would undergo ionization, dissociation, or recombined. Any product atoms would then be tracked through the plasma and can undergo ionization and charge exchange. The particle track terminates upon ionization of the atom. Along the particles' paths, the volumetric source of plasma ions is accumulated in each computational zone. The penetration fraction is then the ratio of the volume-integrated sum of those source rates over zones inside the separatrix to the gas puff rate.

Simplified DEGAS-2 model: While we are interested in conducting this full model study during the 5-yr period, due to present man-power limitations, we have considerably simplified this model to understand a smaller part of the

important gas penetration physics that is relevant to the up-coming NSTX-U MGI experiments. To carry out this simplified study we have used a simple rectangular geometry. In this simplified rectangular geometry, shown in Figure 2.2.3.2.2, a 1m x 1m (in the y and z directions) region is used. Region A represents the SOL region and its width and plasma parameters (density and temperature) can be arbitrarily varied. Region B is the space between the SOL outer edge and the vessel wall. This is 20cm in width and contains no plasma. This width could also be varied to reflect the location of the gas valve with respect to the edge of the SOL. The gas valve, labeled C, is located at the vessel wall.

In present experiments, after the valve opens this gas enters a long drift tube, typically 5 to 10 cm in diameter and about 1- 2m or longer in length. The open end of the tube is positioned to be near the vessel wall. Typical gas flux at the vessel wall ranges from $4E22$ to $7.78E24$ #/cm²/s which covers the range of gas fluxes used in present machines, the upper value being similar to that which may be used in ITER .

The gas pulse width would be specified to be 1ms in duration. As this directed gas plume enters the vacuum region B, it would undergo molecular collisions that would cause the gas to expand and diffuse in the y and z directions. Thus the gas density would decrease as it moves towards the SOL region. The width of this vacuum region and the gas flux magnitude at location C would determine the gas flux in the interface region between regions A and B. Gas molecules that are along the edges of the rectangular mesh (along the y and z directions) are assumed to not penetrate the SOL. Increasing the rectangular mesh dimension to 1.5m in each direction and confirming that the gas penetration fraction does not substantially increase can easily test this. The gas molecules that enter region A would then undergo neutral-neutral collisions, electron-neutral collisions, and ion-neutral collisions. Atoms that are ionized are assumed to be lost along the SOL flows and are assumed not to penetrate past the separatrix. The electron density and temperature in the SOL region would be varied to reflect conditions that exist in the SOL and private flux regions in present machines as well as the anticipated conditions in ITER.

In this simplified model, the SOL and private flux regions can be modeled by varying the length of the dimension A and the corresponding plasma parameters in region A. Thus depending on the choice of the parameters, region A would represent either the SOL or the Private flux region. For instance, to model the NSTX-U SOL, we would use a width of about 0.2 cm for region A and plasma parameters in region A in the range of 10-20 eV and $1-4 \times 10^{18} \text{ m}^{-3}$. Likewise to model the private flux region, the length of dimension A would be increased to span 5 to 10 cm or more, and the plasma parameters in that region correspondingly revised to be similar to the parameters provided under Section 2.2.3.2.1. Again, with the proper choice of the plasma parameters in region A and the chosen length for dimension A, it should also be possible to

obtain estimates for the gas penetration fractions that could be expected in ITER. We plan to complete these simplified DEGAS-2 simulations before Year 2 of NSTX-U operation.

This model would provide a lower bound for the gas penetration efficiency that can then be compared to observed results from DIII-D, C-MOD and other tokamaks. It would also provide guidance for the gas penetration efficiencies for NSTX-U mid-plane and private flux region conditions. Based on the extent of differences between the simplified DEGAS-2 results and experimental observations from present machines as well as from NSTX-U a full DEGAS-2 simulation could be considered during Years 2 to 4 of NSTX-U operations.

These simulations could also be extended to cases where smaller fractions of high-Z gases (neon, argon) are introduced into a carrier He gas to assess the ratio of high-Z to He gas fractions that allow the high-Z component to retain a high velocity. These would be incorporated into the model during years 2 and 3 of NSTX-U operations.

These planned experiments and simulations are expected to contribute to the understanding of important physics questions related to the MGI experiments in support of NSTX-U, ITER and future ST and tokamak based machines. The primary study to be conducted would be to understand the gas penetration efficiency as a function of poloidal gas injection location and variations in plasma parameters, especially at the edge. Supporting DEGAS-2 studies would contribute to quantifying the MGI system requirements aimed at minimizing the gas throughput and maximizing the gas penetration through the separatrix.

2.2.3.2.3 Novel mitigation technologies: electromagnetic particle injector and compact toroid injection development

The compact toroid injection (CT) system is described under Section 4.2.5.3.4, so it will not be discussed here. If installed on NSTX-U, it will be used to test runaway electron suppression in NSTX-U. Runaway electrons can be created during inductive start-up by maintaining a low vessel neutral pressure, and have been generated on NSTX. Safe runaway current start-up scenarios will first need to be developed through a combination of HeGDC wall conditioning, adjusting the pre-fill gas pressure, and optimizing the initial pre-programmed loop voltage ramp so that the runaway current magnitude can be controlled and maintained for 10s of ms in duration. In such discharges, at varying levels of the runaway electron current magnitude, a CT could be injected to test its potential to de-confine the runaway electrons by stochastizing the magnetic field. For comparison, in other similar such discharges, varying levels of neutral gas will also be injected with the MGI system to assess the runaway electron suppression time scales for both methods. Additionally, the results could be compared to results obtained from the use of 3D fields from future non-axisymmetric control coils and existing non-axisymmetric coils to stochastize the magnetic field.

This section describes our on-going work for developing a new system for safely terminating discharges in ITER. The system, referred to as an Electromagnetic Particle Injector (EPI) propels a coaxial projectile, containing particulate matter of various sizes and composition, in a coaxial electromagnetic rail gun, then shatters it in order to inject the smaller sized particles into the tokamak. While experiments on NSTX-U would likely shatter the pellet, the system for ITER may choose to inject the capsule intact. At present this is a design activity that will be completed by December 2012 (This and the statement below will be revised in January, 2013). After that the plans will be discussed with NSTX-U management and the US-DOE to obtain guidance on how to proceed with the next step, which involves fabricating a proto-type injector and testing it off-line during 2013.

At the recent US Disruption Mitigation Workshop (GA, March 12-13, 2012) the following observations were made concerning MGI. First it was agreed that the Massive Gas Injection system is the best understood system for safely terminating discharges in ITER. Second, the time response of this system and the controllability of the amount of gas and impurities injected by this system for variations in the initial plasma current at which a disruption initiates may be inadequate. Third, it may not be possible to fully rely on this system for forced thermal quenches that have less than 10 ms of warning time. Thus, it was agreed that other faster acting systems should be tested and developed. During this meeting, the Univ. of Washington/NSTX groups presented the EPI concept. It was noted that this system was more complex as compared to a conventional gas gun, but no technical flaws were identified. It was also suggested that a proto-type should be built and tested before considering it for ITER.

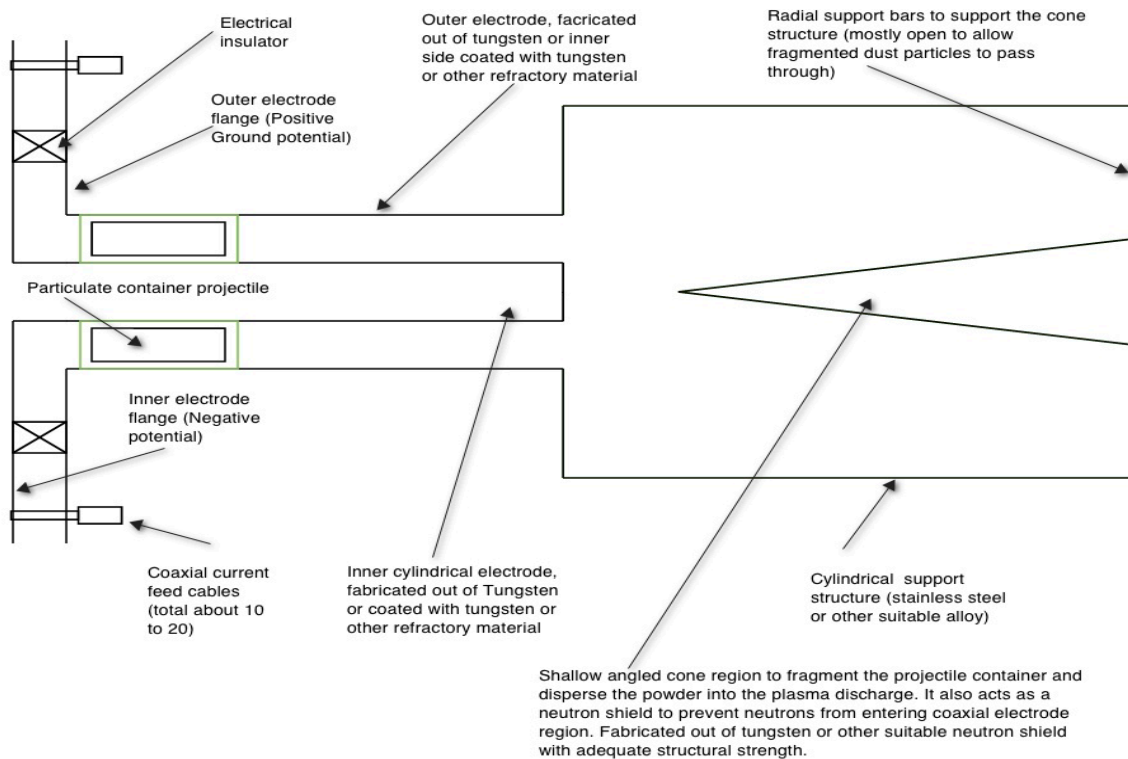
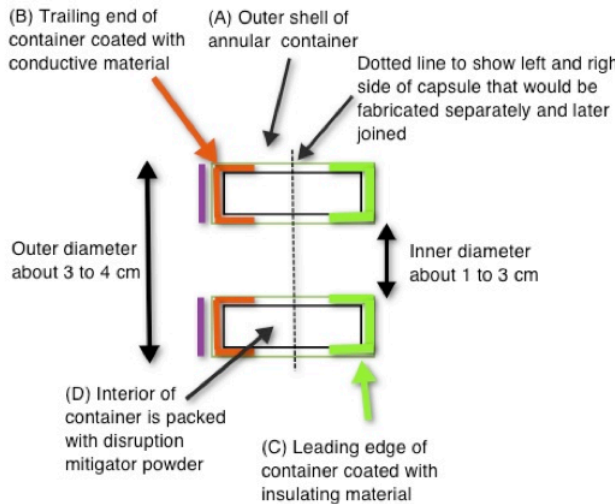


Figure 2.2.3.2.3: Electromagnetic Particle Injector (EPI) using a coaxial electromagnetic rail gun

The proposed system, shown in Figs. 2.2.3.2.3 and 2.2.3.2.3-2, is now under detailed design. It has several advantages over other disruption mitigation systems being considered for ITER. These are:

- It is capable of delivering a highly tailed mass inventory
 - Large particle inventory
 - All particles are delivered at nearly the same time
 - Particles can be tailored to contain multiple elements in different fractions and sizes
 - Tailored particles are fully ionized only in higher current discharges (to control current quench rates)
 - Well suited for long stand-by mode operation
- The toroidal structure and conical disperser ensures that,
 - For smaller machines, the capsule does not enter the tokamak intact

- The capsule will fragment symmetrically and deliver a uniform distribution of particles (or via tapered final Section)
- For larger machines, the capsule can also be injected intact without fragmentation
- Particle penetration is not impeded by magnetic fields



Capsule design

Figure 2.2.3.2.3-2: Shown are the primary elements of the capsule design. The purple ring at the trailing end of the capsule serves two purposes. In an electromagnetic accelerator it is used to increase the inertial strength of the capsule. If the capsule is used in a conventional gas gun it could be fabricated out of a non-conductive material.

- A coaxial rail gun is a fully electromagnetic system with no moving parts, so should have high reliability from long stand-by mode to operate on demand

- Conventional gas guns will inject gas before capsule and will trigger a pre-mature thermal quench

Design studies for NSTX-U have now converged on an attractive and viable system. Table 2.2.3.2.3 contains the specifications for the capsule and injector. The capsule volume would be about 0.5 to 1.5 cm³, as this depends on the packing fraction of the particles within the capsule. For present machines, the capsule would be fabricated out of a thin shell of graphite or the particles could be compression packed with a bonding agent. A similar approach could be used for ITER or a more robust plastic liner could be used to form the capsule.

The purple ring shown in Figure 2.2.3.2.3-2 could be fabricated out of a layer of conductive graphite. For NSTX the capsule would weigh about 3g and contain enough carbon atoms to equal about 20% of the required impurity atom content for a forced thermal quench in ITER. The inner and outer diameter of the accelerator would be 1 and 2cm respectively. The overall injector length would be 20cm for a final velocity of 1km/s. As shown in Figure 2.2.3.2.3-3, which contains results from rail-gun simulations, by extending the accelerator length to 1m, velocities as high as 2km/s could be achieved. The simulations also show that the velocity of 1km/s is achieved in less than 0.5ms after the discharge of the power supply. In systems such as this, it is the power supply that is the high-cost component. Fortunately, because of CHI research on NSTX, the capacitor bank used for CHI research (shown in Figure 2.2.3.2.3-4) is well suited for powering the EPI injector for NSTX-U. The system capacitance is 50mF and it will be operated at 2kV. The RG218 power cables that feed power into the CHI current bus at the

machine would be disconnected and could be connected to the EPI injector bus during disruption mitigation studies.

Capsule Parameters	Injector Parameters
Inner and Outer Radius: 0.5cm and 1cm	Accelerator Length: 0.2 to 1m
Length and Volume: 0.5-1.5cm and 1-3cc	Capacitor bank voltage: 1-2kV
Capsule Mass: 2.8g	Bank Capacitance: 50mF
No. of Carbon atoms: 1.5×10^{23}	Capacitor bank energy: 100kJ
No. of electrons: 9.2×10^{23}	External inductance: 2 μ H
Electrons in capsule/ITER TQ needs: ~ 0.2	Accelerator inductance: $<1\mu$ H

Table 2.2.3.2.3: Capsule and EPI Injector Parameters for NSTX-U

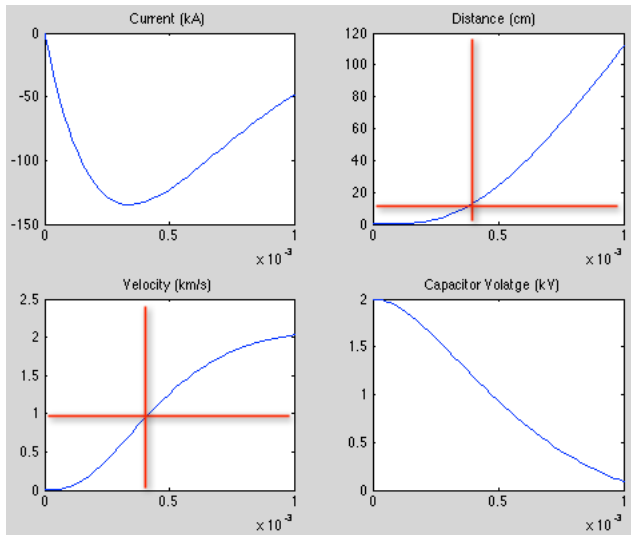


Figure 2.2.3.2.3-3: Results from simulations for the NSTX-U EPI injector. Shown are the accelerator current, capsule velocity, distance traveled by the capsule and the capacitor bank voltage history all as a function of time after discharge of the capacitor bank.



Figure 2.2.3.2.3-4: The NSTX CHI capacitor bank system is well suited to powering the EPI injector for NSTX-U.

During the first year of NSTX-U operations we plan to commission the system by test firing the EPI injector capsule into a NSTX-U plasma discharge. A similar commissioning test will be conducted after a CT system is also installed on NSTX-U.

2.2.3.2.4 Timescale for research in the rapid shutdown techniques topical area

Year 1:

MGI program goals: Test hardware and commission MGI diagnostics

- Using a low triangularity discharge as shown in Figure 1a, we will compare massive gas injection (using a combination of deuterium and helium) of gas injected into the lower X-point and private flux region to that from the vessel mid-plane. This is a comparison of locations 1a and 2 in Figure 2.2.3.2.1a.
- The shape of the plasma will be varied to make it highly triangular so that the outer strike point rests on the inner divertor plate and at a radius less than the radius of the gas injection port (Figure 2.2.3.2.1b). Gas will then be injected into the scrape-off-layer region near the divertor, which is now located in a region of high toroidal field (location 1b in Figure 2.2.3.2.1b). This injection location will be compared to mid-plane injection (location 2, in Figure 2.2.3.2.1b) to understand the effects of gas penetration through the scrape-off layer that is located in regions of high vs. low toroidal field. The same combination of deuterium and helium will be used for these experiments to compare these results to those for the low triangularity discharges.
- During the first year of NSTX-U operations, much of the MGI studies will use a combination of deuterium and helium primarily to gain experience in conducting these studies on NSTX-U for the first time and to commission the diagnostics that will support MGI studies. Towards the end of YR1 operations we will conduct some tests in which neon is introduced as an additional impurity gas in the deuterium/helium gas mix used above to gain experience with the use of high-Z gas and to develop experiments for YR2 that will begin to use high-Z gasses.

Year 2:

MGI program goals: Increase high-Z gas fraction and prepare system for the MGI Milestone for Year 3.

- Based on YR1 results, a desired fraction of neon (in a combination of deuterium/helium carrier gas) will be used for all subsequent comparison experiments to be conducted this year.
- We will compare: (1) the gas transit and system response times, (2) propagation time for the cold front to reach the $q=2$ surface, (3) the amount of gas required for initiating a rapid thermal quench and (4) symmetry of the radiated power profile.

- We will simultaneously inject gas from three locations (bottom, mid-plane and top) to see if a cold mantle could be continually maintained around the disrupting plasma, and assess the benefits of multiple injection location for reducing localized radiation thermal loading.
- Finally, towards the end of YR2 operation, for a chosen condition from the YR2 experiments, neon will be replaced with argon to assess the benefits of each of these gases and to select the gas combination for YR 3 experiments.

EPI program goals: If the EPI system is installed by this time, then the primary objective for the EPI system during Year 2 (but before the end of FY2016) is to assess the EPI injector system's capability to initiate a forced thermal quench in less than 10ms after the system is triggered. This is for assessing its potential to meet ITER needs.

- We will conduct an initial commissioning test of EPI injected capsule into energetic NSTX-U plasma so as to obtain sufficient information to assess its potential as a disruption mitigation system for ITER. Parameters of interest would be (1) time when the projectile particles contact the plasma after system trigger time, (2) time for the resulting thermal quench and (3) reliability of the system. For NSTX-U experiments, the system will be designed to inject the capsule at a velocity of 1 km/s. At this velocity, in principle, the particles should reach the NSTX-U core plasma 3-4 ms after the system is triggered. These initial experiments will be used to guide the capsule velocity requirements for ITER and for YR5 NSTX-U EPI experiments.
- Should the CT system be installed on NSTX-U, a similar such commissioning test will be conducted to demonstrate injection of a CT into a NSTX plasma.

Year 3:

MGI Program goals: Satisfy Milestone 3a (quantify MGI results from NSTX-U). Systems that were installed, tested and improved during the previous two years will this year be used to obtain sufficient quantitative results in support of this Milestone, including the following research tasks:

- Quantify the gas assimilation fraction for variations in the gas injection location and compare to DEGAS-2 modeling results. Assess if a full DEGAS-2 model is required for future work.
- Assess reduction in divertor heat loads and reduction in divertor halo currents for variations in the gas injection location.
- Measure asymmetries in the radiated power profile for variations in the gas injection location and for simultaneous gas injection from multiple locations.
- Obtain additional measurements using the EPI system to assess its benefits over the MGI system.

- If the CT system was commissioned during the previous year, inject a CT into a runaway electron discharge.

Year 4:

Compare MGI and EPI systems in NSTX-U: We will compare characteristics of the thermal and current quench phases for MGI and EPI triggered disruptions.

- Inject MGI at different times into a discharge in which the q-profile is evolving to understand the importance of the location of the q=2 surface to the plasma edge.
- For a high-powered NSTX-U discharge compare the thermal quench rates and the current quench rates for forced disruptions using MGI and EPI.
- We will work with groups using NIMROD, KPRAD, and if possible the EIRENE-SOLPS codes to simulate NSTX-U experimental observations. This is work that will have been initiated during Year 1 of NSTX-U operations.
- Continue to include the NSTX-U MGI and EPI data into the ITER database to contribute to the continued understanding of these systems for ITER, future tokamaks and STs.

Year 5:

Integrate DMS to DM Sensors: Obtain other needed data from the MGI, EPI and possibly the CT systems and to test their reliability to trigger on demand using signals provided by disruption detection sensors in NSTX-U.

- We will trigger the MGI system based on sensor provided data on an impending disruption. Additionally, we will determine if the DM control system is capable of triggering a specific MGI valve based on the plasma configuration (i.e., downward vs. upward moving disruption)
- We will trigger the EPI system based on sensor provided data on an impending disruption.
- The CT system (if installed and tested during previous years) will be used to obtain additional data from discharges that have varying levels of runaway electron current.

See Section 9.2.3.X for additional information of the systems for synthesizing NSTX diagnostic data in order to provide pre-disruption triggers to these systems.

2.2.3.3 Disruption physics

The topic of disruption physics captures a number of topics critical for the reliable operation and design of future tokamaks. In general, these include the physics of:

- transport during the thermal quench, and associated power loading of the PFCs,
- the current quench,
- the generation of halo currents,
- the generation of runaway electrons (REs).

Of these topics, the current quench will be studied extensively in as part of the mitigation research described in Section 2.2.3.2, and will not be addressed here. Due to the strong shaping and lower toroidal field, disruption RE generation is not expected in NSTX-U (the RE studies in Section X are proposed to be done on a RE population generated by low-density Ohmic operation, not disruptions). Hence, the research program described here will focus on the thermal quench and halo current generation.

2.2.3.3.1 Improving understanding of thermal quench physics and transient disruption heat loads

SPG Comment: I am not sure if this can be done in the base budget. It depends whether the cameras would be present I guess.

In the chain of disruption consequences, the first event is the thermal quench. The impulsive thermal loading associated with the quench can lead to severe damage to the plasma facing components. The magnitude of this problem can be viewed in Table 2.2.3.3.1, where the thermal quench heat loads are projected using the methodology from Table 5 of Reference [28]. The pre-disruption thermal energy is used for projecting the thermal loads. The divertor area is taken from Reference [28] for ITER, and as $2\pi R_0 \lambda_{\text{mid}} f_{\text{exp}}$, where λ_{mid} [cm] = $\max(0.2, 1.0/I_p^{1.6})$ [29] and a flux expansion $f_{\text{exp}}=30$ is assumed for NSTX-U and 60 for the next step STs. Furthermore it is assumed that the SOL expands by a factor of 7 during the disruption process, yielding a similar expansion in the wetted area of the divertor. Finally, the time-scale of the heat pulse (τ_{div}) is assumed to be similar to the time-scale of the thermal collapse, and is of order 1 ms. A thermal loading parameter is then estimated as $W/7A_{\text{div}}\tau_{\text{div}}^{1/2}$.

	ITER	NSTX-U	ST-Pilot	Power Reactor
R [m]	6.2	1	2.2	3.2
I _p [MA]	15	2	19	29
l _{mid} [mm]	*	3.299	2.000	2.000
W [MJ]	350	1.5	282	1100
A _{div} [m]	3.50	0.62	1.66	2.41
t _{TQ} [ms]	0.7	0.5	1	1
Loading [MJm ² s ^{-1/2}]	540	15	768	2061

Table 2.2.3.3.1: Disruption thermal loading estimated for ITER, NSTX-Upgrade, an ST-Pilot facility, and an ST power reactor.

The results in the table show that for ITER, a thermal load parameter of roughly $540 \text{ MJm}^2\text{s}^{-1/2}$ is expected, which is much larger than the C or W ablation/melting threshold of $40\text{-}60 \text{ MJm}^2\text{s}^{-1/2}$ [28]. This clearly illustrates why mitigation of the thermal quench is critical for ITER. The NSTX-Upgrade disruption thermal loading is significantly smaller than this threshold, and disruption damage to potential metal PFCs is only expected if the PFC temperature is already significantly elevated. The ST pilot plant, taken from Reference [30] shows thermal loading approximately 30% larger than that projected for ITER. The ST power reactor, whose parameters are loosely based on ARIES-ST, shows thermal loading more than a factor of 5 greater than ITER and 50 times larger than the melting threshold for tungsten, even with the large divertor area generated by running at $f_{\text{exp}}=60$ and a further factor of 7 increase during the disruption.

The research proposed for this area in the NSTX-U research program is based on examining the assumptions made in constructing this table, and then providing an experimental basis for improving them. This process illuminates the key physics assumptions and processes that must be understood to make improved projections to next step STs.

The first physics assumption in these estimates is that stored energy at the time of the thermal quench is equal to the value during the high performance phase. In fact, as shown in Reference [31] for JET and Figure 2.2.3.1.1 for NSTX data [32], there is typically a rather large fractional loss of stored energy in the phase preceding the disruption. For instance, for disruptions in the later flat-top, the most likely case has a stored energy equal to 15-20% of the stored energy at the time of maximum performance. Similarly, Figure 2.2.3.1.1b shows that there is typically a loss of plasma current in the phase leading up to the disruption. Both of these effects can help to mitigate the dangerous aspects of the disruption.

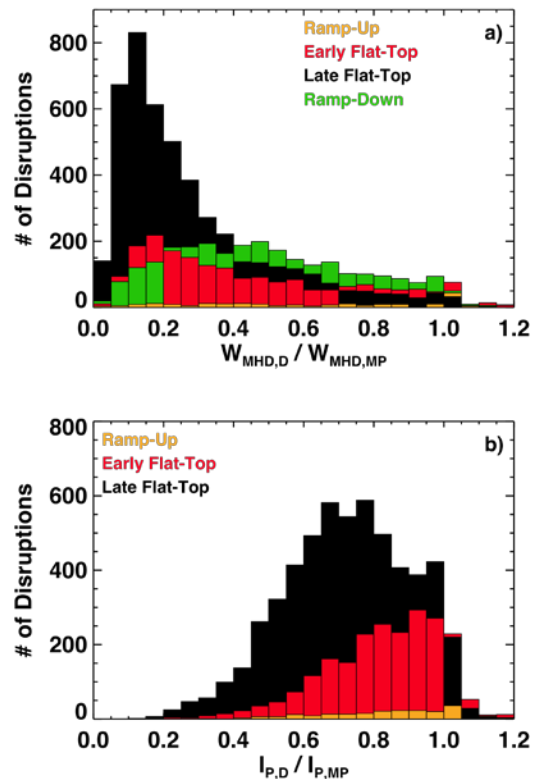


Figure 2.2.3.1.1: Histograms of the pre-disruption loss fraction of a) stored energy, and b) current. The data is broken in the current ramp, the period between the start of flat-top (SoFT) and SoFT+250 ms, the later flat-top, and the rampdown. Figure from Reference [32].

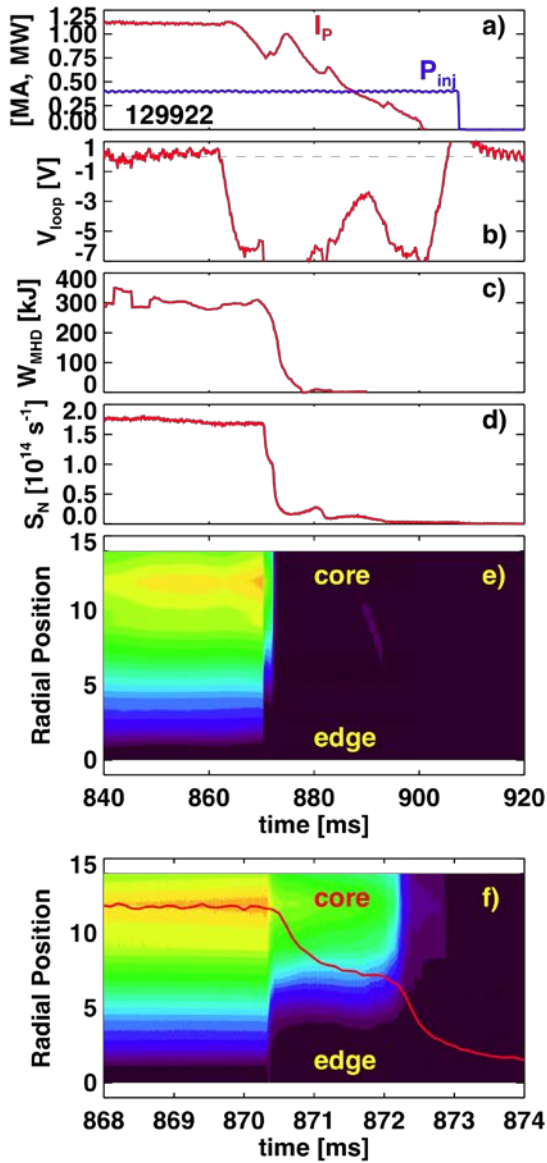


Figure 2.2.3.1.1-2: Time evolution of quantities during a plasma with an extremely rapid thermal quench. Shown are a) the plasma current and injected power, b) the applied loop voltage, c) the stored energy, d) the neutron emission, e) the soft X-ray profile, and f) the neutron and soft X-ray emission zoomed in to the region surrounding the thermal quench. Figure from Reference [32].

increase the levels of pre-disruption energy loss by implementing automated soft-stop procedures, as described in Section 9.2.3.X. This will allow a better understanding of the scenarios under which full-energy disruptions are unavoidable.

Note, however, that there are many examples in Figure 2.2.3.1.1a with minimal fractional stored energy loss preceding the disruption. These cases are often among the few of the highest stored energy disruptions in NSTX. An example of such a disruption is shown in Figure 2.2.3.1.1-2, where frames a) through e) share a common time-base, and frame f) zooms in on the soft X-ray emission dynamics during the thermal quench. In this case, the disruption is triggered by a reversal of the loop voltage in Figure 2.2.3.1.1-2b, as the plasma current is ramped down without first reducing the stored energy. The stored energy of 320 kJ at the time of the thermal collapse is quite large by NSTX standards, and shows no substantial reduction in the phase leading up to the thermal quench. In fact, 21 of the 22 largest stored energy disruptions in NSTX were of this variety, where the loop voltage was reversed during the high performance phase. This observation motivates the ramp-down automation tasks described in Section 9.2.3, designed to avoid this occurrence, but also provides a means to generate reproducible disruptions for physics studies, as will be described in the next Section.

Research in NSTX-U will continue to examine the typical stored energy losses preceding a disruption. More importantly, it is worth noting that the levels of energy loss in Figure 2.2.3.1.1 are only due to natural plasma processes. Collaborative research between the ASC and MS groups will attempt to actively

A second key assumption made in formulating Table 2.2.3.3.1 is that all of the energy present at the time of the thermal quench is conducted to the divertor, and that radiation is not a significant part of the disruption power balance. This assumption will be verified by power balance measurements during disruptions. In particular, the bolometry systems described in Section 2.2.X will be used to assess the total radiation as a function of time, during both the thermal and current quenches. The fast IR thermography systems and eroding thermocouples will be used to assess the heat conducted to the PFC surfaces. Measurements of vessel eddy currents will be used to assess the magnetic energy lost to eddy currents. These measurements will be made for both centered major disruptions and VDE disruptions.

The third assumption in Table 2.2.3.3.1 is with regard to the temporal scale of the thermal collapse and the thermal loading. At conventional aspect ratio, a two-stage thermal quench sequence has often been discussed [28], where there is first flattening of the thermal profiles within the $q=2$ surface, followed by a complete collapse of the remaining thermal energy. The time-scale of the second collapse is used as a worst-case proxy for the time-scale of the thermal loading in the calculation of Table 2.2.3.3.1, though some measurements from AUG [28] indicate that this may be too conservative.

The largest stored energy disruptions in NSTX are also observed to have a two stage thermal collapse. For instance, the neutral emission trace in Figure 2.2.3.1.1-2d shows a two stage collapse, as does the profile of soft X-ray emissivity in Figure 2.2.3.1.1-2e. The dynamics of this two-stage collapse can be seen most clearly in Figure 2.2.3.1.1-2f, where the neutron and X-ray signals have been expanded around the time of the thermal quench. It is clear that, unlike the conventional aspect ratio case, the first collapse occurs at the edge of the plasma. This collapse takes place over 40-60 ms, followed by a nearly constant phase of 1500 ms duration, and the core thermal energy collapse on a time scale of ~200 ms.

The fast IR thermography and eroding thermocouples will be used in conjunction with the core diagnostics to assess the relative timing between the core thermal collapses and the arrival of heat at the divertor surface. These measurements will be conducted for “hot plasma VDEs”, where there is minimal thermal energy loss preceding the vertical motion, and centered disruptions such as that in Figure 2.2.3.1.1-2, where there is minimal plasma motion preceding or during the thermal quench. The presence of multiple time-scales in the thermal collapse will be documented for the various disruption types, and the levels of thermal loading associated with each time-scale will be documented. The effective duration of the thermal energy pulse will be measured, with a view to determine if various effects such as SOL turbulence or plasma sheath effects [28] result in a temporal spreading of the heat flux compared to the time-scale of the core collapse.

The fourth assumption made in assessing Table 2.2.3.3.1 is that the conducted heat flows along the SOL field in a fashion similar to that during the flat-top phase, but with a factor of 7 expansion in the wetted area. Note that significant heat flux is conducted to the inner target during VDEs in DIII-D, by poloidal flows and not fully understood [33]; this effect is potentially more problematic in an ST, given the different divertor areas of the two targets, and must be understood well in order to project for future devices. The IR thermography diagnostics will be used to assess the spatial extent of the conducted heat flux, to determine the correct area expansion factor for estimating thermal loads. Furthermore, the split between the inner- and outer-divertor legs will be assessed, to determine which locations receive the largest energy loading. As with the time-scale studies, these experiments will be conducted in both hot-plasma VDEs and centered, high-energy disruptions.

The fifth and final assumption involved in Table 2.2.3.3.1 involves the assumption of axisymmetry. The axisymmetry of the heat flux could be violated because of helical distortions of the plasma boundary due to MHD activity, or due to enhanced sheath conduction if thermal electron emission occurs on very hot PFC surfaces [34]. This latter effect could be relevant to cases where the PFC temperatures are already highly elevated when the high-energy disruption occurs, and could be strongly localized. Using the proposed wide-angle IR camera view, NSTX-U researchers will examine the disruption heat fluxes for evidence of strong non-axisymmetry, and quantify those asymmetries if present. The dynamics of those asymmetries will be compared to those for the halo currents, which are the topic of the next session.

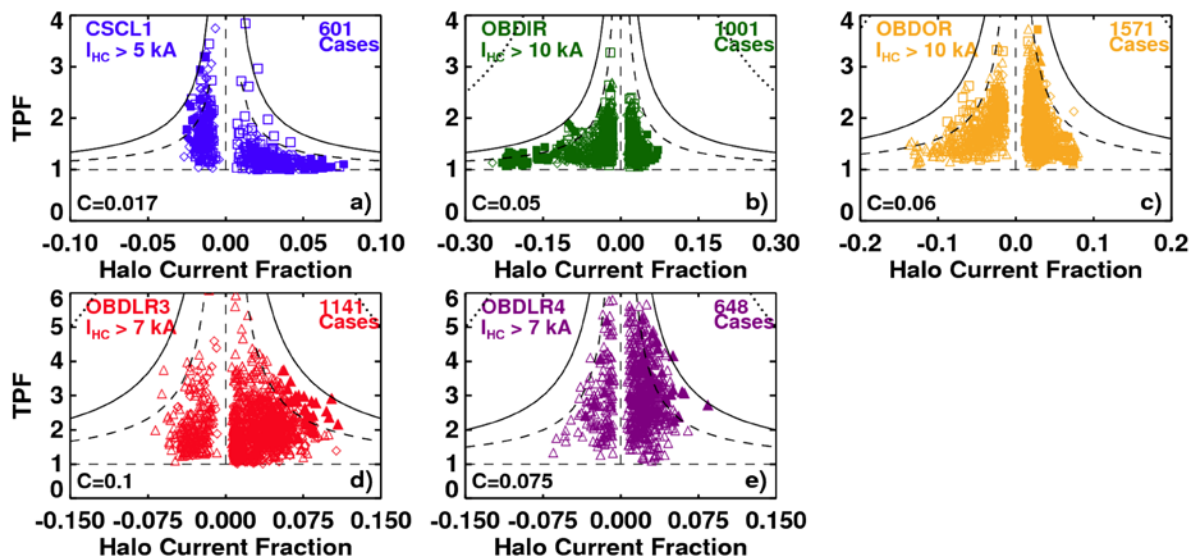


Figure 2.2.3.3.2: Halo current fraction vs. toroidal peaking factor, for a series of diagnostics. Frame a) shows data from instrumentation on the center-stack casing, frames b) and c) show data from the lower vessel wall, while frames d) and e) shows data from arrays of tiles located in the outboard divertor. Figure from Reference

2.2.3.3.2 Improving understanding of disruption halo currents

When vertical stability is lost during the disruption process, the plasma typically moves up or down, and comes in contact with the divertors. Large “halo currents” have been observed to flow from the plasma into the divertor structures, through those structures, and then back into the plasma. The part of this current that resides in the structures, when it flows across the magnetic field, can exert damaging forces on those structures.

Much of the early work on “halo currents” focused on the axisymmetric component of those currents, including their inductive coupling to the main plasma current channel [35]; this case corresponds to the currents being driven by a voltage source. More recent work has emphasized the role of halo currents in reducing the otherwise Alfvénic growth of $n=0$ and $n=1$ instabilities [36,37,34]; the currents in this case act as if they are driven by a current source. Given incremental funding, halo current research in NSTX-U will attempt to understand the relative importance of these two effects, as well as determine more completely the halo current dynamics in a spherical torus. In particular, the goals for halo current research in NSTX-U are as follows:

- Determine the total halo current fraction in next-step relevant ST conditions.
- Better document the toroidal and poloidal structure of the halo currents, and compare to magnetic measurements of the plasma 3D structure.
- Document the reduction of halo currents with disruption mitigation technologies.

These studies will be made possible by a significant expansion of the halo current measurement systems, as described below.

NSTX had a significant array of halo current diagnostics: see Reference [38] for a description of the instrumentation, and Refs. [39,40] for example results. However, even with those extensive measurements, it has been impossible to comprehensively measure the total current flowing in the plasma SOL. This can be understood by examining Figure 2.2.3.3.2, which shows the halo current fraction vs. toroidal peaking factor for measurements at various positions around the NSTX vessel. The largest halo current fractions are measured at the vessel wall in frames b) and c), where values of up to 25% have been measured. However, this measurement must necessarily underestimate the total halo current, on account of the current which can flow along the copper divertor plates, never entering the vessel wall. Frames d) and e) illustrate the total current flowing into a single row of tiles; both the row 3 and row 4 divertor tiles are illustrated. Unfortunately, the total halo width at the divertor floor can be larger than the poloidal extent of these two tile rows, and the sum of the currents in these two rows thus underestimates the total current.

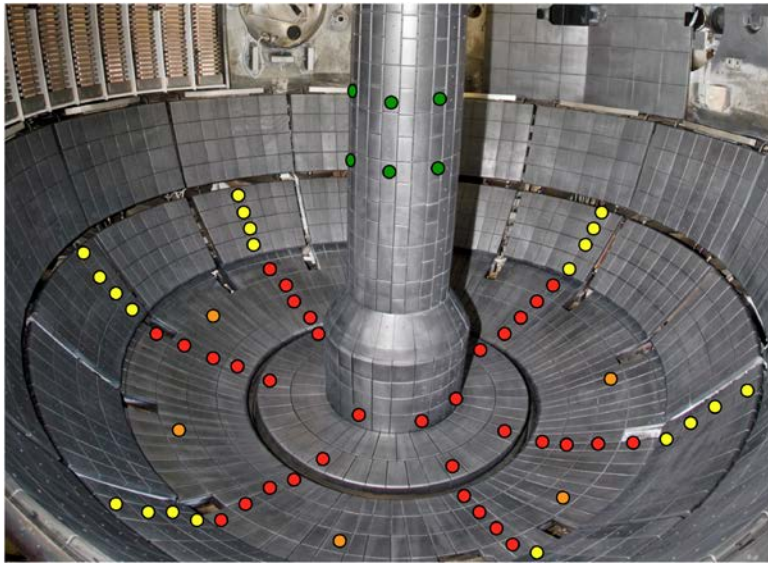


Figure 2.2.3.3.2-2: Proposed expansion of the NSTX-U shunt tile diagnostic set. Each red dot represents a tile which is instrumented with a resistive shunt beneath it. Note that NSTX-U has only a single row of tiles on the inner horizontal target. The colors are explained in the text.

In order to properly measure the total halo current, the shunt tile arrays and other halo current measurements will be significantly expanded. This expansion, indicated conceptually in Figure 2.2.3.3.2-2, will be implemented in a staged way.

For the ST, the most critical location for halo current loading is possibly the center column, since the toroidal field $B_T \sim 1/R$ is strongest there. Hence, measurements during the first year of operation will focus on diagnosing halo

currents at that location, and will utilize an expanded array of sensors on the center column. This includes an array of $12??$ shunt tiles indicated in green in Figure 2.2.3.3.2-2, as well as a toroidal array B_T sensors located near the midplane. The shunt tiles will assess the local halo current density in the central region of the center stack, though they may not be sufficiently dense to measure the total current. This measurement will be accomplished using the array of B_T sensors, which act like segments of a partial Rogowski coil and should be able to accurately assess the total vertical current on the center column (though measurements of the peaking factor by this means will be difficult as per the discussion in [38]). These sensors, along with the total and partial Rogowski coils on the upper and lower portions of the center column, should allow a complete inventory of halo currents on the center column.

The next upgrade to the halo current sensor array will involve improved measurements in the outboard divertor, with the goal of significantly improving the toroidal and poloidal resolution. These will include instrumenting all five rows of the outer divertor, as well as the single row of the inner target, with ~ 6 tiles each; see red circles in Figure 2.2.3.3.2-2 for suggested locations. This toroidal distribution of tiles has proven useful in resolving the approximate toroidal structure of the halo currents in NSTX. We will also consider increasing the toroidal coverage in one or two select rows, in order to better assess any fine structure in the measurement; the arrangement in Figure 2.2.3.3.2-2 shows increased toroidal coverage in the third row of divertor tiles as orange circles.

The final upgrade will involve making measurements of the halo currents on the passive plates. While the most common location for the plasma to limit during a VDE is on the divertor floor, having the plasma limit on the secondary passive plates [39] during a VDE was occasionally observed in NSTX. If this type of VDE continues to occur in NSTX-Upgrade, then the tiles on the secondary passive plates will be instrumented for measurements of currents, as indicated in the yellow circles in Figure 2.2.3.3.2-2. If improvements to the vertical control system described in [Section 9.2.2.X](#) eliminate this variety of VDE, then these tiles will not be implemented

Additional diagnostics will contribute to the understanding of these halo currents. Newly upgraded Langmuir probe diagnostics will facilitate an assessment of the halo electron temperature during the VDE. The new divertor 3D magnetic diagnostics should allow a more precise measurement of the 3D distortions of the configuration during the phase of large currents. These will be used in conjunction with the current measurements to assess the relative phase between the surface distortions and the currents, in order to elucidate the role of the “Hiro current” mechanism in driving these currents. Finally, if the divertor Thomson scattering system is implemented, it may provide a high-quality measurement of the core and halo temperature density during the VDE.

Using the diagnostic systems described above, it will be possible to measure the total halo current density, at the current entrance and exit points, for a wide range of disrupting plasmas. At a basic level, this diagnostic will provide essential data to project global and local halo current to future ST devices. The scaling of the maximum local and global halo currents with plasma current, toroidal field, and VDE characteristics will be documented. However, beyond this simple parameter, the suggested system will target the following physics issues.

We will use the upgraded halo current sensors to assess the poloidal extent of the halo current channel, known as the halo width. This quantity impacts the total resistance of the halo current path, and thus the current that flows when the halo currents are driven as by a voltage source [34]; this drive term was apparently determined to be dominant in MAST measurements [41]. The width of the halo also impacts the spatial region in the divertor over which the force are applied, and is a key input parameter for many halo current simulation codes. Previous measurements in NSTX have been used to make estimates of the halo width [39], but the present system should resolve it more accurately by providing sufficiently broad poloidal resolution.

NSTX-U studies will also assess the toroidal structure of the halo currents. As shown in Figure 2.2.3.3.2-3, previous measurements using six tiles at a fixed poloidal angle showed that the dominant structure of the halo current tended to be a rotating but toroidally localized lobe [40]. In this particular example, the halo currents flow at largely fixed toroidal angle for a ~ 3 ms, then has a period of ~ 2.5 ms where they make 4 complete revolutions around the machine. However,

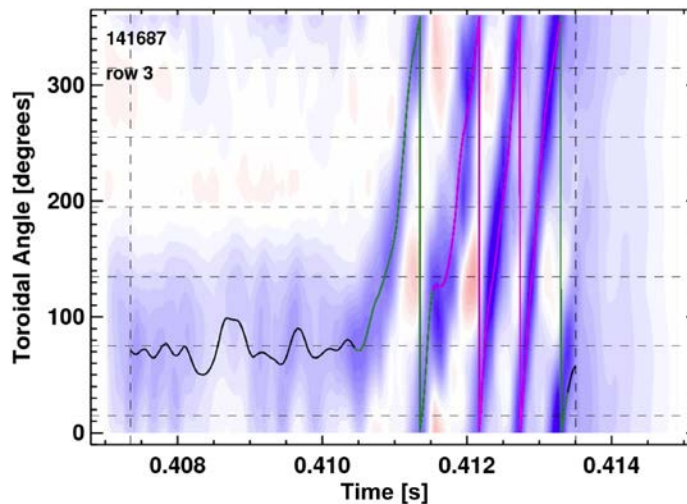


Figure 2.2.3.3.2-3: Evolution of the halo current density as a function of time and toroidal angle but at fixed poloidal angle. Note the strong toroidal rotation of the asymmetry.

previous measurements of the toroidal width of the structure relied on a fitting function that used the intrinsic toroidal rotation of the structure to improve the effective toroidal resolution [40]; the six toroidally distributed tiles were not in general enough to accurately assess the lobe width using the instantaneous data. This resulted in some uncertainty, especially for cases with little or no toroidal rotation. The system indicated in Figure 2.2.3.3.2-2, if it includes the tiles indicated by the orange circles, should be able to accurately resolve the toroidal structure even in the absence of rotation. Understanding the toroidal

structure is critical for determining the potential for severe localization of forces, and can provide key insight into the underlying physics mechanisms generating the currents.

Finally, a key goal of the MGI experiments is to demonstrate a reduction in halo current loading with mitigation. The system described here will be able to comprehensively address this concern, by measuring the total current. With a more sparse measurement set, there is risk that any reduction of current observed with mitigation is simply the result of variations in the VDE dynamics resulting in the location of maximum current moving to a poorly instrumented portion of the divertor.

With regard to the theory of halo currents, there appears to be some consensus that a 3D equilibrium code capable of incorporating the effects of currents in the SOL is required. The development of such a code is beyond the scope of the NSTX-Upgrade experimental program. However, should that activity be pursued elsewhere, the NSTX data collected by this diagnostic system would provide a strong constraint on, or test of, those calculations. The research program described above will also produce data for benchmarking simulations of halo currents using extended MHD codes, as described in Reference [42].

If incremental funding is not provided, it is likely that the halo current diagnostics will be significantly more modest, and will be used to provide limited data for the mitigation experiments. The physics research described above would likely not be completed.

2.2.3.3.3 Impact of operating without solenoid induction on disruption physics

NSTX-Upgrade will be able to operate with 100% non-inductive current drive over a range of field, currents, and heating powers; see Chapter 9 or Reference [43] for additional discussion of this operating space. While many scenarios will continue to use the solenoid for I_p feedback control, it is also possible to deliberately disable that feedback loop. This will then duplicate the capabilities envisioned for next-step STs [44,30,45,46] that do not include an Ohmic solenoid. It is interesting to consider how this modification to the actuator capabilities may modify the disruption characteristics.

Typical H-mode disruptions in NSTX have some precursor modes or event, such as an RWM, locked mode, or H->L transition, that leads to a large drop in stored energy; these are the modes that lead to the large stored energy losses in Figure 2.2.3.1.1. This collapse is typically followed by a 20-100 ms long phase with large loop voltage and, typically, growing vertical instability [32]. The actual thermal and current quenches typically occur only after the solenoid reaches its current limit and begins to ramp down, resulting in a reversal of the loop voltage, or after the plasma is driven into the divertor floor by the uncontrolled vertical motion.

If there were no solenoid induction, the dynamics following the precursor MHD/event would likely be quite different. Rather than responding to the strong inductive edge current drive from the solenoid, the current would begin to decay, though on a time-scale slower than during a true current quench. If the internal inductance were to increase during this process, problems may arise with evolution to unstable current profiles, which could prompt a final disruption. The time available for vertical motion, however, would likely be much less than the cases where induction props up the discharge, and it appears possible that the halo current loading would be reduced in these cases. These various dynamics will be examined in dedicated experiments once 100% non-inductive operations have been established.

2.2.3.3.4 Timescale for research in the disruption physics area

The timeline for this research is provided below. Note that the halo current research described beyond year 1 will likely require incremental funding, due to the expense of installing the shunt-tile diagnostics.

Year 1:

- Investigate halo current loading on the center column, using newly installed center column shunt tiles.

Year 2:

- Upgrade shunt tile diagnostics for complete coverage of the horizontal divertors. Make first assessments of total halo current fraction, toroidal structure, and poloidal width.
- Conduct first experiments on disruption heat loads during VDEs, including studies of spatial extent and timing of the heat deposition.
- Begin assessments of non-axisymmetric heat loading during disruptions, if diagnostic availability permits.

Year 3:

- Extend study of disruption thermal loads to centered major disruptions. Begin efforts to determine the disruption power balance for the various disruption types.
- Complete assessments of halo current scalings using the full field and current capabilities of NSTX-U.
- Conduct experiments examining the impact of fully non-inductive operations, with no loop-voltage feedback, on disruption physics.

Year 4:

- Complete assessments of the disruption power balance for the different disruption types. Complete assessments of 3-D effects in disruptions heat loading
- Utilize upgraded 3D magnetics for comparison of helical distortions and local halo currents.
- Study non-axisymmetric effects on the divertor heat loading.

Year 5:

- Continue support of disruption mitigation experiments by providing data on halo currents and thermal loads. Support halo current and thermal quench modeling activities by providing experimental data.

2.3 Summary of theory and simulation capabilities

<i>Code</i>	<i>Description</i>	<i>Scope</i>	<i>Improvements</i>
EFIT	Equilibrium reconstruction code	Between-shots equilibrium reconstruction	Higher resolution, auto best level, new diagnostics
DCON	Ideal MHD stability code	Ideal Kink stability analysis with and without the wall up to $n=6$	Resistive layer physics across rational surfaces (Resistive DCON)
IPEC/GPEC	Ideal and general perturbed equilibrium with 3D fields	Plasma response, locking, and NTV studies with 3D fields	General force balance equation including general jump conditions
MISK	Modifications to ideal stability by kinetic effects	Calculation of resistive wall mode stability	Improved model of energetic particle, anisotropy effects
POCA	δf guiding-center orbit code	Calculation of neoclassical transport, perturbed pressures and NTV	Improved numerical scheme to enhance computation speed
VALEN	Models currents in structures with thin shell finite elements	Resistive wall mode active feedback simulation	Multi-mode VALEN
MARS-K	Self-consistent kinetic stability calculation	Calculation of RWM stability and plasma response to perturbation	Inclusion of energy dependent collisionality for NTV calculation
M3D-C ¹	Implicit resistive and 2-fluid MHD code	Linear and nonlinear MHD stability	Neoclassical terms, resistive wall being added
DEGAS-2	Monte Carlo code to compute transport of neutral atoms	Calculation of neutral gas penetration through SOL	Include multiple gas species Use exact NSTX-U SOL conditions from UEDGE

Table 2.3: Summary table of the main codes used for theory-experiment comparison on NSTX-U.

2.3.1 EFIT

Accurate equilibrium reconstruction is necessary for experimental analysis as well as input to various other stability codes. In NSTX this capability has been provided automatically between-shots with EFIT [47,48] on two levels: with magnetics only (EFIT01) and with magnetics plus diamagnetic loop plus Thomson electron density and temperature (EFIT02). Additionally, higher levels of reconstruction can be achieved in post-run analysis by including a magnetic field pitch angle constraint from the motional Stark effect (MSE) diagnostic [49] (Section 10.6.1.4). Finally, use of the toroidal plasma rotation (from a charge exchange recombination spectroscopy (CHERS) measurement) is possible. This makes the pressure no longer a flux function, which

complicates the reconstruction. Such reconstructions have been achieved for NSTX, however [50].

Plans for EFIT improvements for NSTX-U operation include the following. Higher time and spatial resolution, from the present typical 5 ms and X points is possible with computer memory improvements. A scheme for automatically detecting the level of diagnostics available and running up to the highest reconstruction level possible (ie with Thomson, or with Thomson plus MSE, etc...) is planned. Finally, new diagnostics that will be available, such as the motional Stark effect with laser-induced fluorescence (MSE-LIF) diagnostic (Section 10.6.1.5), which has the ability to measure both the magnetic field pitch angle, and the magnitude of the magnetic field, $|B|$ [51], will be incorporated.

2.3.2 DCON

Ideal MHD stability is a critical piece of information for plasma operation, as the equilibrium states cannot be sustained or need other passive or active stabilizing mechanism if the stability condition is not satisfied. DCON is the fastest stability analysis code by investigating plasma potential energy only, and is also one of the most precise codes with adaptive radial grids. The DCON application to ideal stability will be continued in NSTX-U, and will be extended to higher toroidal harmonic numbers up to $n=6$, consistent with the plan for high n stability studies in NSTX-U.

DCON is an ideal code, but it also has been developed for application to resistive MHD stability analysis. The so-called resistive DCON has been successful for cylindrical geometry, and will be improved and tested for more general toroidal geometry. The resistive DCON will be very useful to couple and study resistive wall mode and tearing mode physics together in NSTX-U.

2.3.3 IPEC / GPEC

The ideal perturbed equilibrium code (IPEC) has been successfully applied to study the basic feature of plasma responses to small 3D fields in tokamaks. The code utilizes the Euler-Lagrange equation in DCON to solve the ideal force balance and couples solutions to the external 3D field. Various external coils in different devices, NSTX-U, DIII-D, KSTAR, JET, ITER are implemented and IPEC results will be applied to study error field thresholds for locking, plasma response, and neoclassical toroidal viscosity. Recently calculations of neoclassical toroidal viscosity have been implemented into the IPEC code, based on the combined NTV formula

without large-aspect-ratio approximation, which will enable us to study NTV more precisely in NSTX-U.

Although the ideal plasma responses are often dominant, non-ideal forces such as NTV torque can modify the 3D equilibrium itself. The general perturbed equilibrium code (GPEC) is under development to incorporate such non-ideal forces in a self-consistent way, as well as more generalized jump conditions across the rational surfaces beyond the ideal constraints. The GPEC code will be highly useful to study plasma responses to 3D fields especially in high-performance plasmas above the no-wall limit and also to investigate the interactions between 3D plasma responses and inner-layer activities when successfully developed.

2.3.4 MISK

The MISK, or Modification to Ideal Stability by Kinetic effects, code [52] calculates the change in potential energy of the plasma due to kinetic effects, δW_K . Along with the fluid δW terms calculated using a marginally stable eigenfunction with the PEST code [53], the dispersion relation or energy principle including kinetic effects is used to predict the growth rate of the resistive wall mode. This approach assumes that kinetic effects do not change the eigenfunction, and that the mode growth rate and frequency are small, so their nonlinear inclusion is unimportant. Cases which are above the ideal no-wall limit, and therefore would be unstable without kinetic effects, are examined. MISK has been used extensively (see Refs. [54,55,9,56,8,57,58,59]) and good agreement between the theory and experimental trends have been found.

2.3.5 POCA

POCA (Particle Orbit Code for Anisotropic pressures) is a newly developed δf particle code to calculate neoclassical transport, perturbed pressures, and NTV in perturbed tokamaks using the δf Monte Carlo method [7]. Every kind of guiding-center motion is tracked by Hamiltonian orbit equations, and the Fokker-Planck equation is solved with a momentum-conserving pitch-angle scattering collision operator. POCA was successfully benchmarked with neoclassical theories, and verified $1/v$, $v_{\perp} v^{1/2}$, superbanana plateau regimes, and bounce-harmonic resonances in NTV transport. Good agreements in NTV torque were also obtained with magnetic braking experiments of DIII-D and NSTX [60]. POCA will be extensively used to predict and analyze the non-axisymmetric field effects on neoclassical transport.

2.3.6 VALEN

VALEN was created to simulate magnetic feedback in resistive wall mode (RWM) problems. The passive growth rate of such an instability is reduced by the interaction of the growing magnetic field from the plasma instability with the conducting structure. The changing magnetic field from the plasma instability produces electrical currents in the conducting structure. The magnetic fields from these induced currents reduce the passive growth rate of the instability. The growth rate of the instability can also be changed by additional magnetic fields produced by electrical coils in a negative feedback. In order to simulate such a problem VALEN models conducting structures, sensor coils, active control coils, power supplies, a feedback logic and the basic instability.

VALEN models currents in distributed structures with a thin shell finite element integral formulation. Every surface is described by a mesh of 3-sided or 4-sided elements. Each element behaves as an individual electromagnetic object, and is coupled with all other elements in the model. This formulation describes the current distribution in terms of circulating loops of current. This approach is a generalization of ‘mesh analysis’ used by electrical engineers to analyze simple circuit problems.

2.3.7 MARS-K

MARS-F/K (Magnetohydrodynamic resistive spectrum – Fluid/Kinetic code) is a toroidal MHD-kinetic hybrid stability code [61,62] that has been benchmarked with IPEC, MISK and HAGIS codes. The code solves the eigenvalue problem derived from the linearized single-fluid ideal/resistive MHD equations with toroidal flow, self-consistently including the drift kinetic effects in full toroidal geometry. The approach allows the kinetic effects associated with the thermal or energetic particles to consistently modify the mode eigenfunction, which could significantly influence the mode stability and structure in certain circumstances [63,64]. The code simulates a plasma surrounded by a pure vacuum region, includes a set of radially separated, toroidally complete resistive walls and a set of magnetic coils located in the vacuum region. With these features, MARS-F/K has been successfully applied to physical study and support of experiments on various subjects such as MHD instabilities (e.g. resistive wall mode and tearing mode), and plasma response to external fields (e.g. resonant field amplification and resonant magnetic perturbation).

The MARS-K code has been modified to include the actual collisional frequency with energy dependence and will be used to study perturbed equilibria by including kinetic effects self-consistently. The upgraded MARS-K and the newly developed quasi-linear version MARS-Q

will be applied to the calculation of self-consistent kinetic stability and neoclassical toroidal viscosity for NSTX-U plasmas.

2.3.8 M3D-C¹

The M3D-C¹ code [65,66] represents a complete rewrite of the older M3D 3D MHD code. It can be run as resistive MHD or two-fluid MHD, and also can be run as either 2-variable or 4-variable reduced MHD. The code is fully implicit using the split-implicit method and this enables it to take large time steps and run to long time. It uses high-order finite elements in 3 dimensions. These elements force the function and its first derivative to be continuous (C1-Continuity). This property allows spatial derivatives up to 4th order to be treated when using the Galerkin method. This property is essential for an implicit formulation using the potential/stream function form of the velocity field and magnetic vector potential. Current emphasis is on modeling sawteeth, snakes, ELMs, and the seeding of NTMs. Future work will be to treat NTMs including neoclassical effects, and to include a resistive wall.

2.3.9 DEGAS-2

DEGAS-2 [22,67,23] uses Monte Carlo techniques to compute transport of neutral atoms and molecules in the vicinity of material surfaces; general three-dimensional devices can be modeled.

Neutral transport in fusion devices is computed using a Monte Carlo technique in general three-dimensional geometries. DEGAS-2 has been designed as a state-of-the-art code featuring optimized geometry / tracking, dynamic memory allocation, and built-in parallel processing. General methods for handling atomic and surface physics data have been developed to make physics modifications easy. Linear and nonlinear neutral elastic scattering processes have been included. The code is designed to be run in a coupled fashion with fluid plasma codes, as well as in a stand-alone mode. It is intended to be portable with thorough documentation.

DEGAS [68] is the predecessor to DEGAS-2. It uses the pseudo-collision algorithm for scoring, as opposed to the track-length estimator in DEGAS-2. The former works better in a dense plasma; the latter in a vacuum. Unlike DEGAS-2, the surface and atomic physics interactions are hard-wired into the code and are difficult to modify.

DEGAS-2 has been verified against multiple analytic and semi-analytic models. It has been thoroughly compared with original DEGAS and EIRENE, and comprehensively validated

against NSTX gas puff imaging experiments. Comparisons with various Alcator C-Mod experiments have been undertaken, but not completed.

2.4 Summary of diagnostics for macroscopic stability research

Diagnostics critical to macroscopic stability research plans in NSTX-U are described in this section. In some cases the diagnostic is described in far more detail elsewhere (Chapter 10, for example), in which case only a brief description and a pointer to that section is provided.

2.4.1 Magnetic B_P and B_R RWM sensor upgrade

A possible upgrade to magnetic poloidal and radial RWM sensors (described in Section 10.6.3) would include the same number of toroidal positions as the present RWM sensors, but closer to the divertor region. This would allow mode measurement closer to the divertor region, based on the theoretically expected large amplitude of high beta $n = 1$ single mode, and the $n = 1$ multi-mode there. This upgrade would also factor in directly to the RWM state space controller.

Other applications of such an upgraded sensor set include:

- Measuring the magnetic signature of Hiro/Halo currents.
- Measuring the MHD at the injector during CHI.
- Measuring SOL current filaments and ELMs.

Several considerations must be accounted for, however, including the optimal sensor polarities, effective areas, integrator/digitizer schemes, and the schedule for divertor upgrades that might mandate removing those sensors

2.4.2 Real-time velocity measurement for successful implementation of rotation control, and disruption detection

A real-time velocity diagnostic, which is integral to macroscopic stability research because of its use in rotation control and disruption detection, has already been installed in NSTX and is described in detail in Section 10.6.3.

2.4.3 Toroidally displaced multi-energy SXR to study 3D physics including island dynamics, and RWM eigenfunctions

A system of two toroidally displaced, edge and core in-vessel tangential multi-energy soft X-ray arrays is proposed to study 3D physics including island dynamics, RWM eigenfunctions, and enhanced sensitivity non-magnetic toroidal mode identification for disruption sensing. This system is described in detail in Section 10.6.1.3.

2.4.4 Core X-ray imaging spectrometer to study rotation effects on error field and early MHD without NBIs (Delgado)

(Add text here)

2.4.5 Internal magnetic fluctuation measurement for island structures (Yuh)

(Add text here)

2.4.6 Real time MSE and MPTS for fast and precise kinetic equilibrium reconstruction

Real-time motional Stark effect and Thomson scattering diagnostics are generally useful for macroscopic stability research through improved equilibrium reconstruction. These systems are described in detail in Sections 10.6.3.1 and 10.6.3.2.

2.4.7 Diagnostics for disruption mitigation studies

Diagnostic shunt tiles for halo current measurements have already been described in the context of disruption physics studies in Section 2.2.3.3.2.

As noted in Section 2.2.3.2, a critical component of the disruption mitigation process is the radiation of nearly all the plasma stored energy. It thus follows that this very large and potentially toroidally asymmetric radiation should be measured, using soft X-ray and bolometer diagnostics.

The present SXR system on NSTX consists of three arrays: two poloidal viewing arrays, and a tangential mid-plane multi-energy array [69,70]. The Johns Hopkins University (JHU) group plans to support disruption mitigation experiments with these diagnostics. The existing poloidal arrays on NSTX are similar to the SXR arrays used on DIII-D for disruption mitigation

experiments.

Because the thermal quench (TQ) phase could be highly non-symmetric it is desirable to have views from three or more toroidal locations. Because the plasma parameters during MGI experiments are quite different from normal plasma operations it is highly desirable to have dedicated diagnostic for disruption mitigation experiments. Furthermore, both the existing poloidal systems are single energy systems. It is desirable to have three energy bands to monitor the plasma simultaneously during the TQ, and hence a multi-energy system is beneficial. The

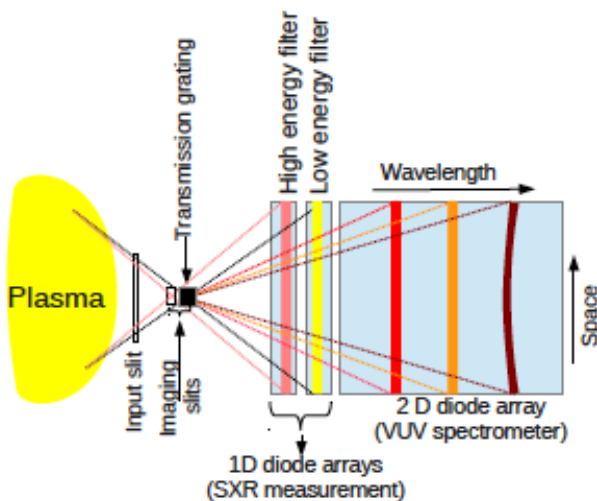


Figure 2.4.7: Cartoon of the SXR/VUV diagnostic for NSTX-U disruption mitigation studies

JHU group has conducted a conceptual design study of the DM diagnostic. The SXR part of the diagnostic being considered is similar to the Multi Energy-SXR array on NSTX.

Figure 2.4.7 shows a cartoon of the proposed diagnostic for disruption mitigation experiments. The diagnostic combines a multi-energy (dual-energy shown in the figure) soft x-ray (SXR) system, and a transmission grating based imaging VUV spectrometer. A pinhole like arrangement of the input and imaging slits restricts the view of the detectors to a poloidal cross-section of the plasma. A transmission grating placed next to the imaging slit diffracts the radiation to produce spectrally resolved one-dimensional images of the plasma on the 2D diode array detector. The impurity line radiation during current quench (CQ) is expected to be in the VUV range (200-1400 Angstroms), and is expected to be sufficiently bright [71] so that the spectra can be measured by a 2D array of diodes at a rate of ~20 kHz. Diodes have been used for the detection on transmission grating based spectrometers in space [72,73] and pinch plasmas [74], but the use of 2D diode arrays will be a novelty. Diode array based detection is expected to provide impurity assimilation measurements during CQ, an essential ingredient in modeling the runaway electron population at the end of the quench, if it should occur on NSTX-U. The other part of the diagnostic is a set of filtered 1D diode arrays similar to the multi-energy soft x-ray system developed for NSTX [70]. Note that the SXR arrays will have separate systems of input and imaging slits. The collapse of the electron temperature during massive gas injection experiments is already studied using filtered SXR diodes on DIII-D and Alcator C-Mod [24,75]. However, the schematic described here will allow a compact diagnostic with multiple energy bands all sharing the same view of the plasma.

If these multi-energy diagnostics should prove infeasible due to cost constraints, we will explore simpler systems for monitoring the total level and toroidal asymmetry of the radiated power. Examples of such systems include that implemented on C-Mod, where diodes with vertical slit “pinholes” were used to measure the total radiated power in toroidally-thin cross-sections of the plasma at multiple toroidal angles.

2.5 Non-axisymmetric control coil (NCC)

2.5.1 Motivation and design

The powerful utility of 3D fields has been rapidly appreciated in tokamak research community, as 3D fields can provide selective channels of transport and thereby stability control. As 3D fields can break toroidal symmetry, the modification of toroidal rotation is the most apparent target of 3D field applications. However, it is important to achieve flexible applicability since stability is not a simple function of rotation, and also depending on the instability rotational shear can be more influential. Also 3D fields can produce particle transport and provide particle control when they are sufficiently resonant with a local region, as well-known by ELM modifications by resonant magnetic fields (RMPs). The RMP results, however, have demonstrated a wide spectrum of utility, as essentially all different devices showed slightly or largely distinct modification of ELMs. The complexity of 3D field effects are perhaps not so surprising as 3D fields entirely opens one additional degree of freedom in plasma shaping, but the present understanding and predictability are highly insufficient for successful applications in next-step devices. The non-axisymmetric control coil (NCC) is fully aligned with the common goal of 3D field physic research, with much wider and presently unprecedented flexibility of field spectrum in space. The physics of resonant magnetic perturbations, including stochastization, turbulence, and rotation shear changes can be explored with the NCC.

The NCC is best justified by recognizing how NSTX-U can uniquely investigate the associated physics. For example, NSTX-U will uniquely operate in non-inductively driven plasmas. This major operational regime may require greater control, and provides a unique lab to test NCC advanced stability physics. Also, NSTX-U will uniquely explore the high beta ST operational space. This allows us to perform advanced stability control using NCC in operating space where disruptivity is not maximized at the highest β_N , or β_N/I_i .

Another important goal of the NCC is to generate an environment relevant for the next-step devices, such as ITER or FNSF. The presently designed RMP coils, or error field correction (EFC) coils, in ITER have three rows of coils, including midplane and two off-midplane coil sets. NSTX already has the midplane coils, which will be further exercised with the 6 independent SPAs, and thus the NCCs are designed with two off-midplane coil sets, as shown in Figure 2.5.1. Figure 2.5.1 shows in fact the 4 possible forms of NCCs, paired by upper and lower set of coils. The set closer to the midplane is the primary option, and the other is the secondary option. They can be installed in the front of the passive plate (Blue) or at the backside (Magenta).

The NCC has 12 toroidal arrays because it is important to explore higher n , up to $n=6$, which can give faster attenuation of the field strength from the edge to the core and better selectivity for edge control. Also, it is desirable to have the rotating capability for $n=3$ and $n=4$, which are presently chosen as primary control fields for ITER ELMs, as the rotating field can be detectable in various static diagnostics and so their 3D structure can be fully measured.

The design of the NCC must also address such practical, engineering matters as: mounting, cooling, power supplies, vacuum feedthroughs, and impact on disruption loads.

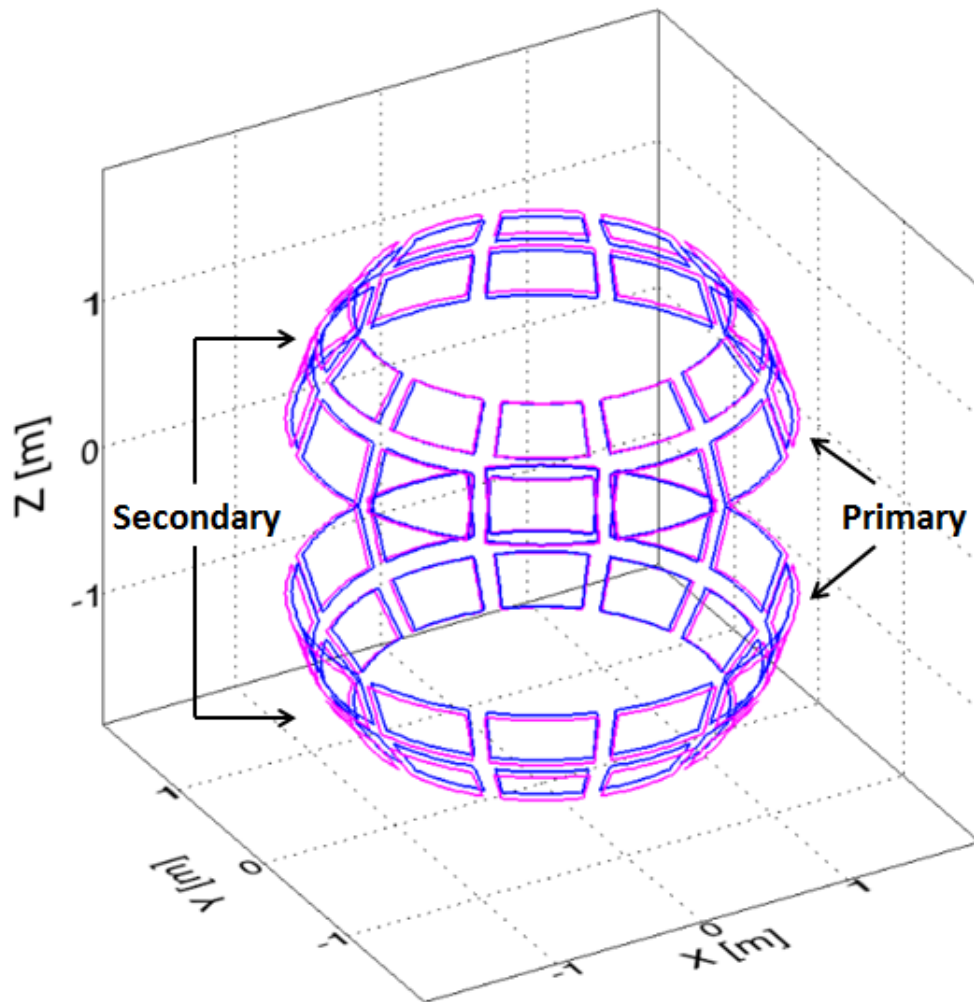


Figure 2.5.1: The 4 possible forms of NCC coils. Paired by upper and lower set of coils, there are primary and secondary options depending on the proximity to the midplane, and also depending on the location relative to the passive plate (Blue and Magenta).

This chapter will describe our research efforts with the designed NCCs, on important topics including RWMs, NTV braking, error field correction, and ELM control and stabilization. First NSTX-U target plasmas are produced with TRANSP, and various field spectra including $n=1-6$ are applied to illustrate the utility of NCCs. Figure 2.5.1-2 shows the $n=1-6$ stability without the wall for NSTX-U target plasmas as a function of β_N , which is important to perform 3D equilibrium calculations. Ideal equilibrium calculations are more reliable for stable plasma, so $n=2-6$ was applied to $\beta_N = 3.5$ and $n=1$ was studied separately with lower $\beta_N = 2.5$. Results can be extended to higher β_N , as experiments have shown the 3D field effects are applicable beyond the no-wall limit, often monotonically. The limitation of ideal calculations needs to be improved, including kinetic particle effects in the future.

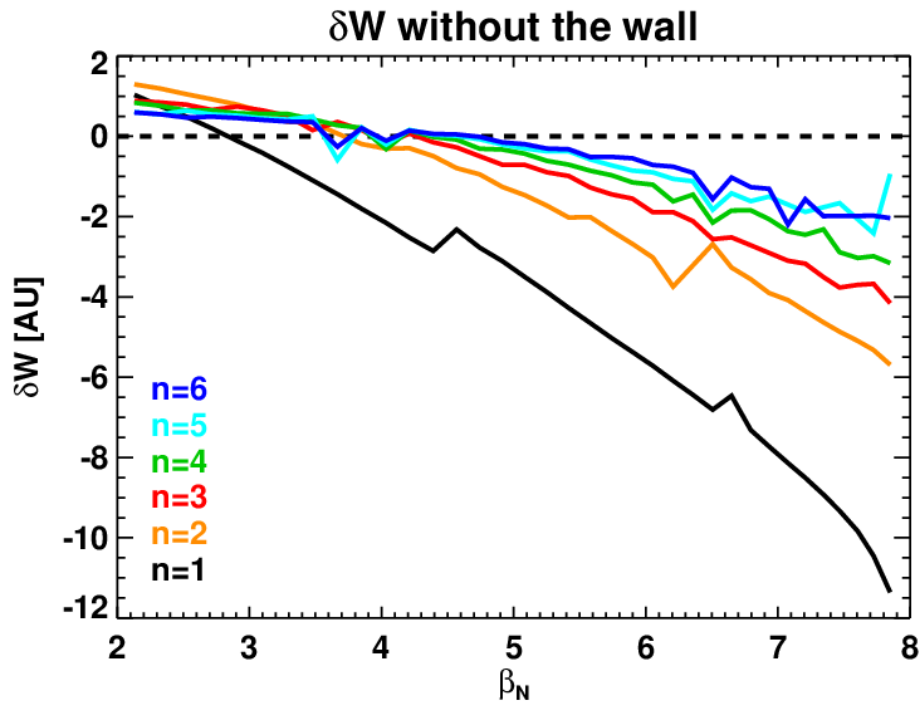


Figure 2.5.1-2: The $n=1-6$ stability of NSTX-U target plasmas without the wall as a function of β_N .

2.5.2 Summary of physics studies

2.5.2.1 RWM active control for significant multi-mode spectrum

-

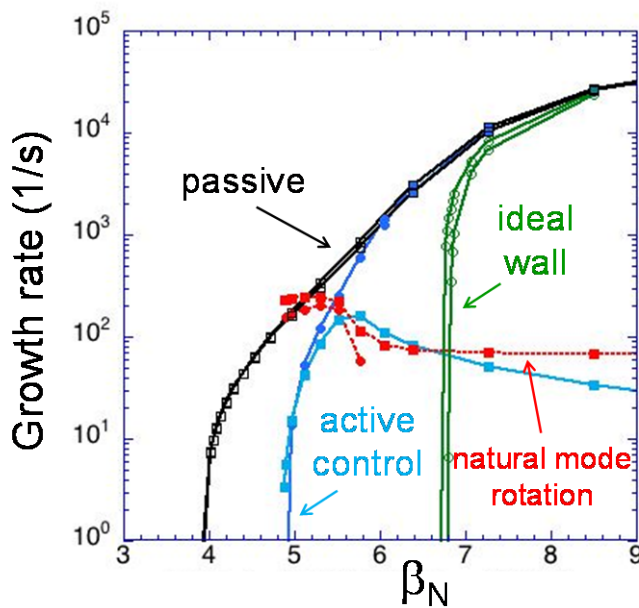


Figure 2.5.2.1: xxx

The NCC will be extremely useful in the area of RWM active control. Calculations with the VALEN code indicate that the X option for the NCC coils can provide active RWM control to achieve β_N near the $n=1$ ideal wall limit (see Figure 2.5.2.1).

Additionally, the NCC will be used in combination with a model-based RWM state space controller, providing multi-mode RWM control and dynamic error field correction (DEFC) with an observer. The RWM state-space controller allows a far greater flexibility of global mode stabilization physics studies with these coils,

with a relatively simple control software upgrade. We will be able to demonstrate RWM state space control of ITER-similar coil set in NSTX-U.

The NCC can provide quantitative evaluation of the importance of the multi-mode spectrum (n and m) for RWM control and DEFC. The $n > 1$ mode spectrum has been observed but the importance of control / dynamic correction has never been tested. We will evaluate what can be gained from $n=2-3$ RWM active control. Also the spectrum will gain helicity, which is important to expand the research.

Finally, the NCC will be instrumental in two additional topics of RWM control. First, we can investigate the physics and control of “nonrigid” mode evolution. Second, an important practical topic for ITER is how to prepare to compensate 1-2 random coil failures in RWM active control. The combination of NSTX-U’s RWM state space controller and the flexibility of the NCC allows us to address this issue.

2.5.2.2 Rotation control by NTV braking

A major topic of interest with the NCC will be NTV physics, and v_ϕ control (with $n \leq 6$). A strong, precise, controllable NTV effect has been observed in NSTX. Open-loop v_ϕ profile

alteration is not routinely performed on other devices, offering a unique capability. There is even the possibility of increasing v_ϕ via $n > 1$ toroidal propagation that can be explored with the NCC.

The flexibility of the field spectra from the NCC will be dependent on power supplies. First it is assumed that all the coils carry the same current, which can be easily produced even with a single power supply. In this case the variation of the poloidal field spectrum is different depending on the toroidal mode number. There are 12 possible phase shifts between the upper and lower set of coils for $n=1$, and the number of possible combinations is reduced to 6, 4, 3, 2, for $n=2, 3, 4, 6$, respectively. Figure 2.5.2.2 shows the total NTV torques achievable using the $n=3$ 1kAt, for the primary (Red) and for the secondary (Blue) option of NCCs, installed in the front of the passive plates. The P1-4 stand for the phase shift between upper and lower set of coils, subsequently increased to the counterclockwise from the upper to the lower set. One can see the primary option can provide the greatest flexibility of NTV compared to the present RWMEF coils and the secondary option, almost by an order of magnitude.

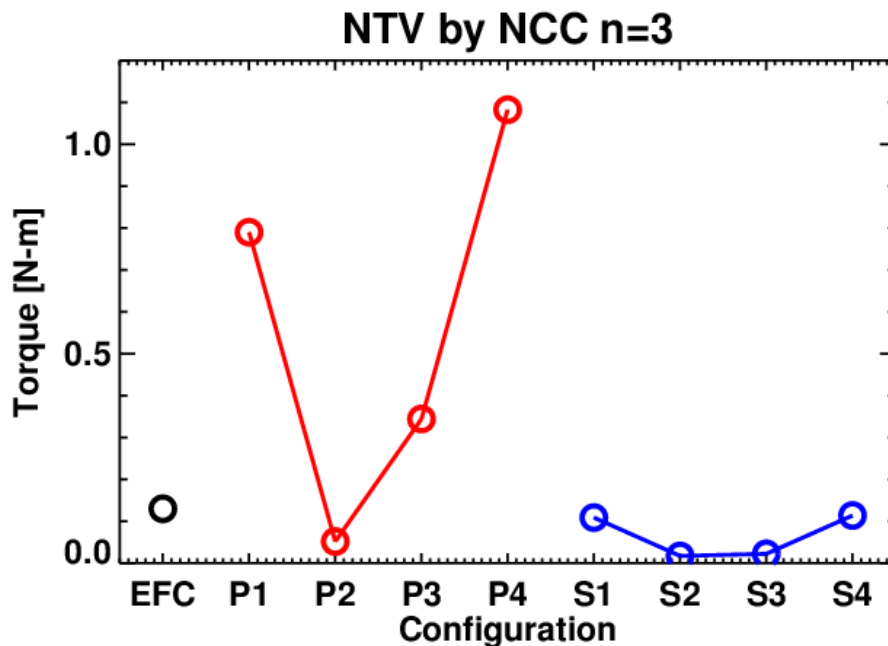


Figure 2.5.2.2: The $n=3$ NTV by each present EFC, the primary (Red) and the secondary (Blue) options with 1kAt and with 4 different phase-shift between upper and lower set of coils.

The difference in capability can be seen more apparently when the NTV torque profiles are examined, as shown in Figure 2.5.2.2-2. The NTV torque profiles by the primary option are

coded by red colors. Compared to the NTV profile by EFC (Black), one can see that the primary option can provide much better selectivity for the edge to the core. That is, the primary option can provide larger NTV in the edge by an order of magnitude and smaller NTV in the core by an order of magnitude at the same time, if the phase shift is optimized.

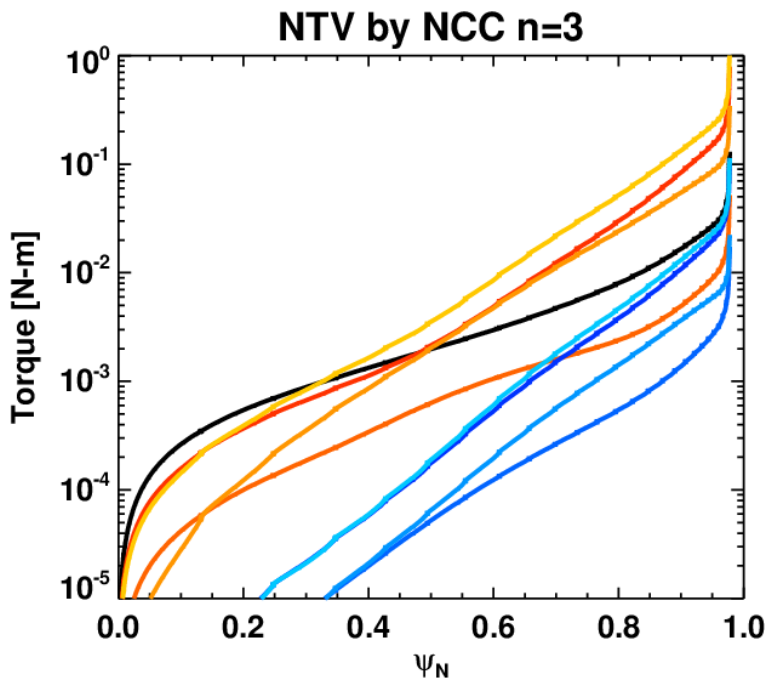


Figure 2.5.2.2-2: The NTV torque profiles, integrated from the magnetic axis, by the $n=3$ NCC fields by 1kAt. The red lines are for the primary option, the blue lines for the secondary option, and black is for present EFC.

The selectivity of the edge vs. the core can become even stronger by an order of magnitude if higher $n>3$ fields are utilized by NCC coils. Figures 2.5.2.2-3 and 2.5.2.2-4 show the NTV torque profile by $n=4$ and $n=6$, as color coded in the same way as Figure 2.5.2.2-2, for the primary and the secondary option.

(Needs to be combined with Chirikov)

2.5.2.3 Error field stabilization

The NCC can also provide much higher flexibility of the $n=1$ field, which will be useful for error field correction as well as RWM control. Figure 2.5.2.3 shows the NCC capability in producing the $n=1$ δB_{21} resonant field depending on the 12 different phase-shifts between the upper and lower sets of coils, for the primary option (Red) and for the secondary option (Blue), compared to the present EFC (Black), by 1kAt. The $n=1$ PF5 error field when PF5 coil currents are 20kA is also shown (Green). One can see the various helical pitches can be produced by NCC coils, which can be flexibly used for optimal error field correction.

(Tearing mode stabilization?)

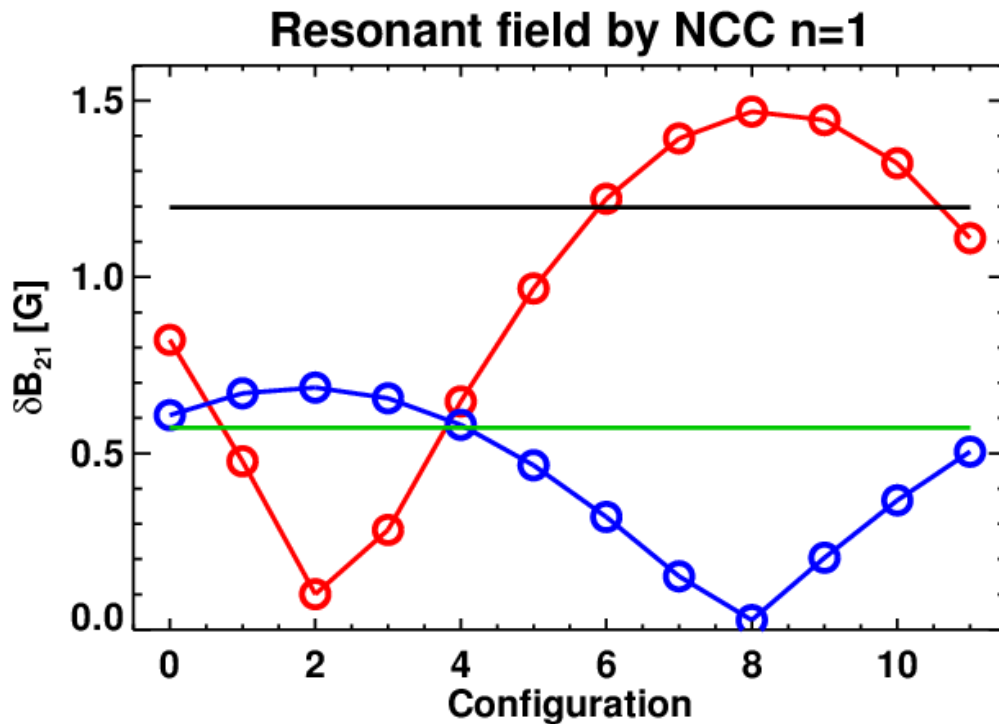


Figure 2.5.2.3: Resonant field at $q=2$ that can be produced by NCC coils by 1kAt, with the primary option (Red), and the secondary option (Blue), compared to the present EFC (Black). The resonant field by PF5 coils with 20kA is also shown, which needs to be minimized by error field correction.

2.5.2.4 RWM kinetic stabilization

Studies of RWM kinetic stabilization physics can be enhanced by the NCC by exploring such issues as:

- What are the optimal rotation profiles for RWM kinetic stabilization?
- Can an optimized NCC field spectrum change edge fast ion profiles for RWM stability alteration?

These topics would be explored experimentally and compared to theoretical calculations using the MISK code.

2.5.2.5 ELM control and stabilization

The proposed NCC coils in NSTX will have great capability in the area of ELM control and stabilization. In high δ , κ double-null plasmas, $n=6$ fields from the NCC could produce a wider edge stochastic layer than $n=3$ I-coil fields in DIII-D, over a wider range in q_{95} (i.e., $5.3 \leq q_{95} \leq 12.8$). Combined $n=6$ and EF/RWM $n=3$ field line loss fractions could exceed those due combined $n=3$ I-coil and $n=1$ C-coil fields in DIII-D. Also NSTX-U with the NCC may be the only machine that could rotate $n=3$ perturbations smoothly to smooth out heat flux to the divertor. Many topics of physics study in this area are possible, including:

- What level of the temperature control can be achieved when the 3D fields can be flexibly rotated? Divertor IR analysis could address this issue.
- What is the stochastic transport physics of the Chirikov parameter getting larger and larger above unity?
- What is the physics of transport barriers that prevent the inner stochastic field lines from getting out and hitting the wall?
- ELM mitigation techniques typically cause density pumpout, but is this really necessary? Can we manipulate the shape of the pedestal profiles?
- What is the field spectrum and strength required for ELM mitigation and ELM suppression, including very high-performance targets? TRIP3D can be used to illustrate the difference in the pitch-alignment and Chirikov overlap. IPEC can be added to show plasma response characteristics.
- We do not yet understand the physics of why energy, particle and momentum transport are very different in L-mode plasmas than in H-mode plasmas. In particular, energy transport in RMP L-mode plasmas dominates particle transport while in H-mode plasmas particle transport is dominant. What is the underlying physics mechanism responsible for switching the dominate transport channel for heat to particles as we go from L to H-mode? High m,n coils will give us new information on this important issue.
- For higher n RMP fields coils need to be optimized to weight the poloidal mode spectrum towards much higher m components. A preliminary vacuum field study done with TRIP3D indicates that window frame coils with a smaller aspect ratio (i.e., toroidal arc length over poloidal arc length) improves the high m weighting ($m=qn$ so for example $q=3$, $n=6 \rightarrow m=18$ while for $q=6$, $n=6 \rightarrow m=36$). The advantage of higher m,n RMP fields is that they are expected to produce smaller “screening” currents (according to 2 fluid MHD theory). The trade-off is that more RMP coil current is needed to increase the high m spectral components as the aspect ratio is reduced. So developing an effective high m,n RMP window frame coil is an important step for understand and testing screening theory as well as other aspect of RMP physics.

These topics constitute a rich, meaningful and unique research plan in the area of ELM control and stabilization in NSTX-U with the NCC. They will help improve our understanding of RMP physics and increase our confidence in the proposed ITER ELM Coil design

2.5.2.6 Simultaneous control for rotation, error field, RWM, TM, ELM

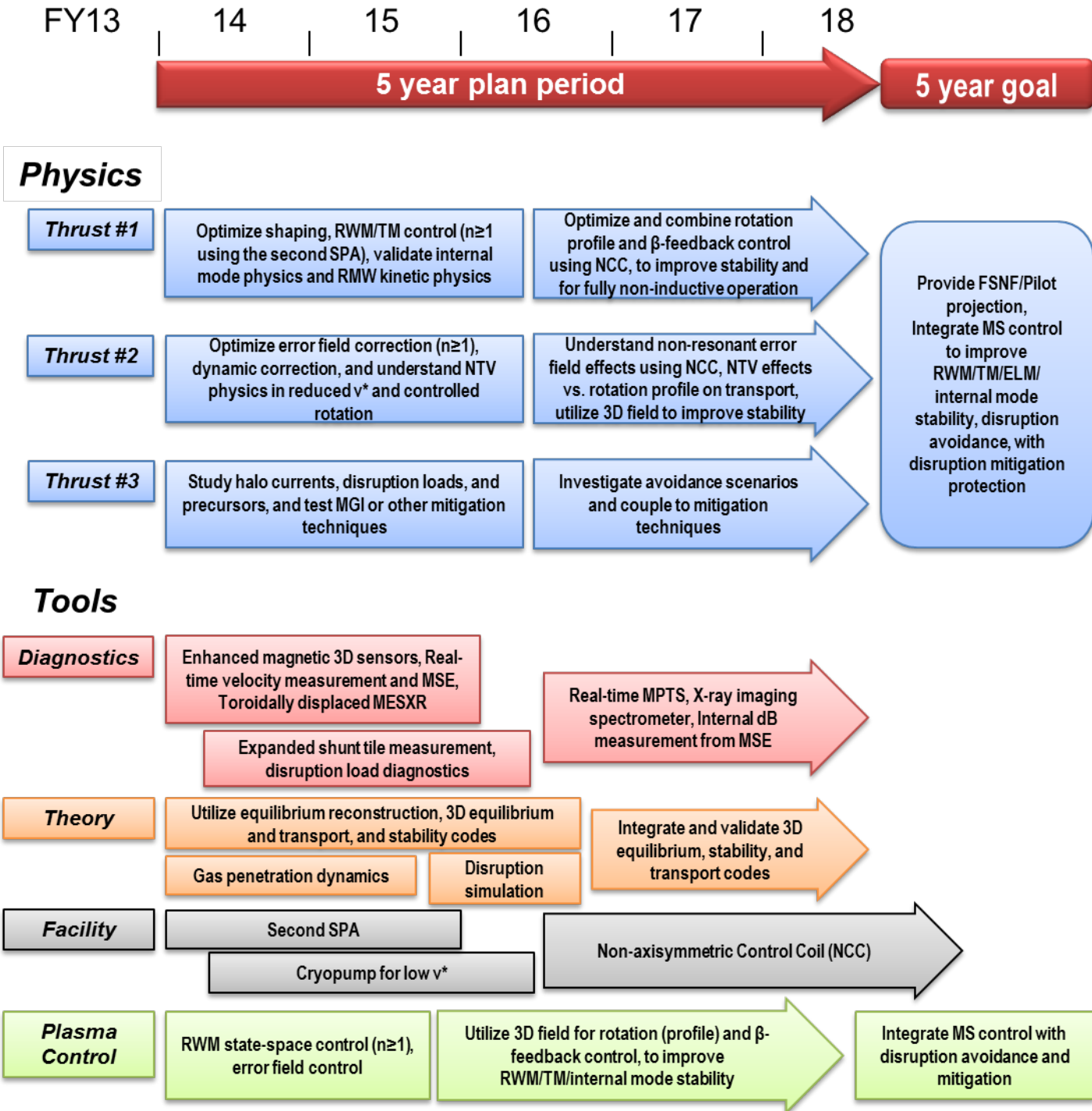
The proposed NCC can be used to demonstrate simultaneous use of actuators sharing multiple control roles. In other words, can the proposed NCC achieve RWM control, ELM control, rotation control, and error field correction simultaneously? Exploring this unique physics coupling in control systems is key for ITER. For example, RWM and TM stability depend on v_ϕ , q , n , and T profiles, while v_ϕ control will depend on NTV (which itself depends on v_ϕ , q , n , and T profiles). The NCC may improve such control. A control model must be tested that utilizes the NCC in coupled systems: for v_ϕ control, β_N control, RWM control (and passive stability), and dynamic error field correction.

2.5.2.7 Prediction for ITER and FNSF 3D coil capabilities

Several questions pertaining to future devices can be addressed with the NCCs in NSTX-U, including:

- Is the integrated controllability largely changed in fully non-inductive operation?
- FNSF might require vertical position control to be performed by internal coils such as these. This can be tested in NSTX-U with the NCC.
- Demonstration of ELM suppression in a fully non-inductive scenario is needed for FNSF.

2014-18 Macroscopic Stability Research Timeline



References

- [1] J.-K. Park, et al., Phys. Rev. Lett. **99** (2007) 195003.
- [2] S.P. Gerhardt, et al., Plasma Phys. Contr. F. **52** (2010) 104003.
- [3] J.E. Menard, et al., ITER Task Agreement #C19TD22FU, "The study of the error fields using Ideal Perturbed Equilibrium Code (IPEC)" (2010).
- [4] W. Zhu, et al., Phys. Rev. Lett. **96** (2006) 225002.
- [5] J.-K. Park, et al., Phys. Rev. Lett. **102** (2009) 065002.
- [6] S. Satake, et al., Phys. Rev. Lett. **107** (2011) 055001.
- [7] K. Kim, et al., Phys. Plasmas **19** (2012) 082503.
- [8] J.W. Berkery, et al., Phys. Rev. Lett. **106** (2011) 075004.
- [9] J.W. Berkery, et al., Phys. Plasmas **17** (2010) 082504.
- [10] J.E. Menard, et al., Nucl. Fusion **50** (2010) 045008.
- [11] D.G. Whyte, et al., J. Nucl. Mater. **363-365** (2007) 1160
- [12] G. Pautasso, et al., Plasma Phys. Contr. F. **51** (2009) 124056.
- [13] E.M. Hollmann, et al., Phys. Plasmas **17** (2010) 056117.
- [14] D.G. Whyte, et al., Fusion Sci. Technol. **48** (2005) 954.
- [15] C. Reux, et al., Nucl. Fusion **50** (2010) 095006.
- [16] P. Lang et al., Phys. Rev. Lett. **79** (1997) 1487.
- [17] R. Maingi et al., Plasma Phys. Contr. F. **46** (2004) A305.
- [18] V. Kotov, D. Reiter and A.S. Kukushkin, "Numerical study of the ITER divertor plasma with the B2-EIRENE code package," Bericht des Forschungszentrums Julich, Jul-4257, November (2007)
- [19] S.L. Allen, Rev. Sci. Instrum. **68** (1997) 1261.
- [20] A.S. Kukushkin, et al., Nucl. Fusion, **47** (2007) 698.
- [21] D.L. Rudakov, et al., Nucl. Fusion, **45** (2005) 1589.
- [22] D.P. Stotler and C.F.F. Karney, Contrib. Plasm. Phys. **34** (1994) 392.
- [23] D.P. Stotler, et al., J. Nucl. Mater., **363-365** (2007) 686.
- [24] V.A. Izzo, et al., Phys. Plasmas, **15** (2008) 056109.
- [25] T.D. Rognlien, et al., Contrib. Plasm. Phys. **34** (1994) 362.
- [26] T.D. Rognlien, et al., J. Nucl. Mater. **266-269** (1999) 654.
- [27] D.P. Stotler, et al., Contrib. Plasm. Phys. **50** (2010) 368.
- [28] T.C. Hender, et al., Nucl. Fusion **47** (2007) S128.
- [29] T.K. Gray, et al., J. Nucl. Mater. **415** (2011) S360.
- [30] J.E. Menard, et al., Nucl. Fusion **51** (2011) 103014.
- [31] V. Riccardo, et al., Nucl. Fusion **45** (2005) 1427.
- [32] S.P. Gerhardt, et al., "Disruptions, Disruptivity, and Safer Operating Windows in the High-b Spherical Torus NSTX", submitted to Nuclear Fusion (2012).
- [33] E. Hollmann, private communication.
- [34] A.H. Boozer, Phys. Plasmas **19** (2012) 058101.
- [35] D.A. Humphreys and A. G. Kellman, Phys. Plasmas **6** (1999) 2742.
- [36] L.E. Zakharov, Phys. Plasmas **15** (2008) 062507.
- [37] L.E. Zakharov, et al., Phys. Plasmas **19** (2012) 055703.
- [38] S.P. Gerhardt, et al., Rev. Sci. Instrum. **82** (2011) 103202.
- [39] S.P. Gerhardt, et al., Nucl. Fusion **52** (2012) 063005.

-
- [40] S.P. Gerhardt, et al., “Characterization of the Disruption Halo Current Toroidal Asymmetry in NSTX”, submitted to Nuclear Fusion (2012).
- [41] G. Counsell, et al., Plasma Phys. Contr. F. **49** (2007) 435.
- [42] J. Breslau, et al., “MHD Calculation of halo currents and vessel forces in NSTX VDEs”, paper PP8.00017, APS-DPP, Providence, RI (2012).
- [43] S.P. Gerhardt, et al., Nuclear Fusion **52** (2012) 083020.
- [44] Y-K M Peng, et al., Plasma Phys. Contr. F. **47** (2005) B263.
- [45] F. Najmabadi, et al., Fusion Eng. Des. **65** (2003) 143.
- [46] H.R. Wilson, et al., Nuclear Fusion **44** (2004) 917.
- [47] L.L. Lao, et al., Fusion Sci. Tech. **48** (2005) 968.
- [48] S.A. Sabbagh, et al., Nucl. Fusion **41** (2001) 1601.
- [49] F. Levinton, et al., Rev. Sci. Inst. **70** (1999) 810.
- [50] S.A. Sabbagh, et al., Nucl. Fusion **46** (2006) 635.
- [51] E.L. Foley, et al., Rev. Sci. Inst. **79** (2008) 10F521.
- [52] B. Hu, et al., Phys. Plasmas **12** (2005) 057301.
- [53] R. Grimm, J. Greene, and J. Johnson, “Methods in Computational Physics, Vol. 16,” (Academic Press, New York, 1976) Chap. Computation of the Magnetohydrodynamic Spectrum in Axisymmetric Toroidal Confinement Systems, pp. 253-280.
- [54] B. Hu, et al., Phys. Plasmas **13** (2006) 112505.
- [55] J.W. Berkery, et al., Phys. Rev. Lett. **104** (2010) 035003.
- [56] S.A. Sabbagh, et al., Nucl. Fusion **50** (2010) 025020.
- [57] Y.S. Park, et al., Nucl. Fusion **51** (2011) 053001.
- [58] H. Reimerdes, et al., Phys. Rev. Lett. **106** (2011) 215002.
- [59] J.W. Berkery, et al., Phys. Plasmas **18** (2011) 072501.
- [60] K. Kim, et al., “Study of neoclassical toroidal viscosity in tokamaks with a δf particle code and resonant nature of magnetic braking,” Proc. 24th Int. Conf. on Fusion Energy (San Diego, USA, 2012) (Vienna: IAEA) paper TH/P2-27.
- [61] Y.Q. Liu, et al., Phys. Plasmas **15** (2008) 112503.
- [62] Y.Q. Liu, et al., Plasma Phys. Control. Fusion **52** (2010) 104002.
- [63] J.E. Menard, et al. “The role of rotation and kinetic damping in high-beta ST plasma stability”, Proc. 39th EPS Conf. 2012, P1.061
- [64] Z.R. Wang, et al., Phys. Plasmas **19** (2012) 072518.
- [65] N.M. Ferraro, et al., Phys. Plasmas **17** (2010) 102508.
- [66] N.M. Ferraro, et al., Phys. Plasmas **19** (2012) 056105.
- [67] D. P. Stotler and B. LaBombard, J. Nucl. Mater. **337-339** (2005) 510.
- [68] D. Heifetz, et al., J. Comp. Phys. **46** (1982) 309.
- [69] D. Stutman, et al., Rev. Sci. Inst. **70** (1999) 572.
- [70] K. Tritz, et al., Rev. Sci. Inst. **83** (2012) 10E109.
- [71] E.M. Hollmann, et al., Nucl. Fusion **48** (2008) 115007.
- [72] D.L. Judge, et al., Sol. Phys., **177** (1998) 161.
- [73] R. Viereck, et al., “Solar extreme ultraviolet irradiance observations from GOES: design characteristics and initial performance,” Proc. SPIE 6689, Solar Physics and Space Weather Instrumentation II, 66890K (September 20, 2007)
- [74] L.E. Ruggles, et al., Rev. Sci. Instrum., **72** (2001) 1218.

[75] D.G. Whyte, et al., “Studies of requirements for ITER disruption mitigation systems,” Proc. 22nd Int. Conf. on Fusion Energy (Geneva, Switzerland, 2008) (Vienna: IAEA) paper IT/P6-18.